Behavior of Individual Pulverized Asphaltenes in a Tube Furnace under Inert Atmosphere

by
Satarupa Dhir

A thesis submitted in partial fulfillment of the requirements for the degree of

Master of Science

in

Chemical Engineering

Department of Chemical and Materials Engineering
University of Alberta

Abstract

Oil sands found in Athabasca and Cold Lake regions of Northern Alberta form Canada's primary source of energy reserves. Asphaltenes, a significant part of bitumen is often considered to be the least valuable component of crude oil due to various factors such as difficulty in transporting and processing. However, utilization of asphaltenes plays a crucial role in overall economics of oil sands extraction. Gasification of asphaltenes can result in much needed hydrogen for upgrading of bitumen. Pyrolysis is the first step in gasification that directs formation of soot on one hand and char formation on the other. However, very limited study has been carried out on pyrolysis of asphaltenes in entrained bed conditions. Single particle investigations are useful since they are conducted in a well-controlled environment allowing elimination of complexities arising from particle-particle interactions.

In this work, pyrolysis of pulverised Asphaltenes feedstock was carried out in a drop tube furnace (DTF) maintained in atmospheric pressure. Effect of furnace temperature and particle size on char formation and char characteristics were investigated. Chars obtained from higher particle size (1.7mm to 0.85mm) at 600˚C, 700˚C and 800˚C exhibited similar morphology to that of pure asphaltenes while pyrolysis of particle sizes ranging from 250-425μm at higher temperatures (700-900˚C) demonstrated better results with 10-2% volatile matter remaining in char. SEM as well as cross sectional images of char particles indicated formation of cenospheres and fragmentation of char particles at higher pyrolysis temperatures. High pyrolysis temperatures also implicated loss of active sites,

increase in alkene content and aromatic condensation. ICP MS investigation validated retention of K and Na along with heavy elements such as V, Ni and Cu at temperatures above 700°C. Morphology of char obtained at different oxygen partial pressures was also examined. Ultimately, the combustion reactivities of char obtained at 700°C, 800°C and 900°C for particle sizes 425μm-0.85mm, 355-425μm and 250-355μm were compared.

Acknowledgements

When I joined University of Alberta, I had limited experience on design of experiments and research. But it was with relentless support and motivation of my supervisor Dr. Rajender Gupta extended during conduction of experiment that made completion of task possible. One of the humblest persons I have ever known, his continuous advice, encouragement and patience steered the project to receive credible research data. I am highly indebted to him for providing me an opportunity to work as an independent researcher and spiking my quest for answers.

I would extend my gratitude to Mr. Nirlipt Mahapatra without whose help the design and assimilation of the setup would have been impossible. I highly appreciate the assistance extended by Dr. Mehdi Mohammadalipour during the analysis of data. His deep understanding on several characterization techniques helped me to obtain reproducible results. I am also thankful to Dr. Deepak Pudasainee and Dr. Moshfiqur Rahman for thoroughly revising the SOP and risk assessment form and making the course of my experiments hazard free and safe.

My experimental work would have been incomplete without the help of wonderful and highly competent technicians Mr. Nathan Gerein and Mr. Guangcheng Chen. I highly appreciate the customer care and service provided by Swagelok personnel Mr. Andrew Worthington. I would also like to thank my friend Natalia Sanchez for assisting me in using the FTIR facility in her research group.

I also owe my gratitude to Mr. Pramod Sripada for helping me understand the working of furnace and providing precious insight into process implementation. I would also take this opportunity to thank my friends Madhudi, Vinoj, Sahil, Olawale and Rishik for their constant support and invaluable suggestions during the course of experiments and thesis formatting.

I also acknowledge the financial support provided by Nexen Energy ULC., Canadian Centre for Clean Coal/Carbon and Mineral Processing Technologies (C_5MPT), Helmholtz Alberta Initiative (HAI) and Natural Sciences and Engineering Research Council of Canada (NSERC).

Finally, I would thank the most important persons in my life, grandma, grandpa, parents and sister for their belief in me even in the dullest phase of life. Special thanks to my grandma for supporting and nurturing me right from the time of birth. It is her faith and blessings that has made me strong and passionate about achieving dreams.

Contents

List of Figures

List of Tables

Chapter 1
INTRODUCTION

1.1. Oil Sands Overview

Oil sand is composed of quartz sands that are enveloped by bitumen film. Each grain is surrounded by layers of water and then bitumen oil. The angular shape of grains and tendency to stick to one another makes the oil sand abrasive and difficult to handle. Oil sand is alternatively called “tar sands” or “bituminous sands”. Bitumen is solid at 10˚C while increase in temperature during summer makes it soft as molasses. Some bitumen is present within 200*ft* while most are deeply buried. Bitumen content in mining pit varies from 18% to 1% while low content areas are not worth mining.

1.1.1. Location

Venezuela and Canada are few of the countries that have oil reserves in the unconventional form of oil sand. Most of the deposits are exclusively mined in northern Alberta, Canada predominantly around three zones: Athabasca, Peace River and Cold Lake area. Athabasca oil sand is the largest among these areas spanning an area of 93,000 km^2, centered on northern town of Fort McMurray. The Cold Lake area covers 18,000 km^2 while Peace River area is around 29,000km^2 [1]. The Alberta Crown owns 81% of mineral rights and is managed by Alberta Department of Energy. The remaining 19% are held by Federal Government within Aboriginal reserves, by the railway companies and by descendants of original homesteaders[2].

1.1.2. Recovery

Depending on the depth oil sand is recovered by open-pit mining and in situ drilling. Approximately 20% of oil sand lies close to earth’s surface for open pit mining. Open-pit mining is similar to coal mine operations where large shovels are utilised to remove oil sands. The oil sand is mixed with water and transported through pipeline for bitumen separation. The remaining recovery of oil sands is

done by in situ drilling method which involves steam assisted gravity drainage (SAGD). This method involves pumping steam underground through horizontal well to liquefy bitumen which is pumped out through secondary well. Less popular in situ drilling called cyclic steam stimulation may also be used. In this method steam is pumped in vertical well to liquefy bitumen and pumped back to surface through the same well.

1.1.3. Production and Economy

Increase in global energy demands calls for an increase in all forms of energy conventional (oil, coal, natural gas, nuclear) or unconventional (oil sand, oil shale, biomass According to IEA report, the global demand will rise by 33% in 2035 with China and India being the major consumers[3]. With demand rising worldwide and declining conventional resources there will be a need to secure the supply of energy through unconventional resources. Canada has the 3rd largest reserve of oil in the world after Venezuela and Saudi Arabia. Figure 1.1 indicates the position of Canada in terms of oil supply globally. Most of reserves are in form of unconventional oil i.e. oil sand. Of the 173 billion barrels of oil that can be recovered economically about 137 billion barrels are concentrated on oil sand[2]. Oil sand production, both upgraded and non-upgraded is expected to increase from 1.98 million barrels per day (2013) to 3.7 million barrels per day (2020). With political stability and robust infrastructure provided by Canada, the global partners would have an advantage importing energy from this country. According to Canadian energy Research Institute (CERI), almost all the sectors are affected by developments in oil sand industry. The oil sand currently provides 149,000 direct jobs across Oil sand investment , re-investment and operating revenues have an GDP impact of $3,865 billion dollar in Canada[2].

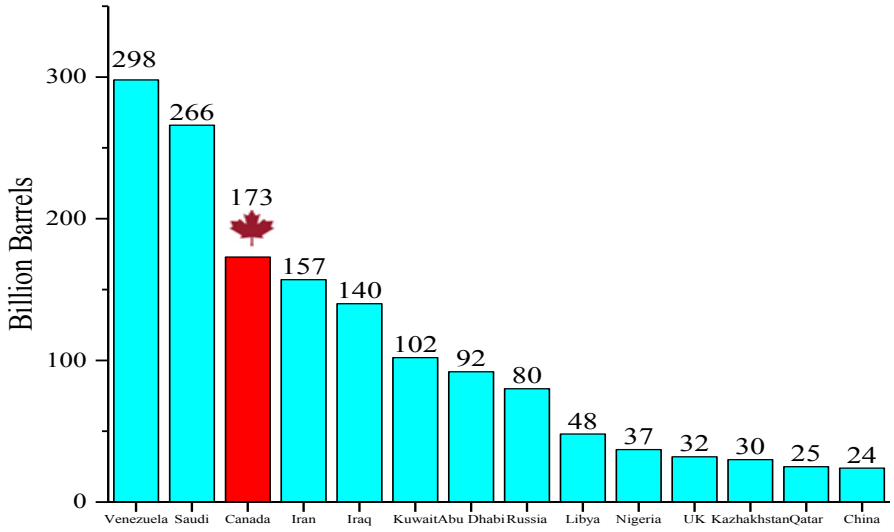

Figure 1.1: Oil reserves in world [2]

1.1.4. Impact on Environment

Increased development in oil sand upgrading and refining over last few years have drawn interest on the environmental impacts of the currently operating as well as future projects. Upgrading and refining of oil sands is an energy intensive process. All steps produce Greenhouse gas (GHG) emissions such as CO_2 which is a major contributor to climate change. Oil sand companies along with collaborations from universities and research institutes have been able to reduce GHG emissions by 30% for every barrel of oil sand crude.

Oil sand operations such as seismic activities, tailing ponds, pipelines, wells, access roads contribute to impact on the landscape. Any oil sands mine has 25-50 year life span while the in situ operations run for 15 years. The land reclamation activity is still in early stages of development and companies are evolving their technologies to reduce impact on land[4]. Wapisiw Lookout is Suncor's first tailing pond to be successfully reclaimed and has been diversified to sustain boreal forest and various species.

Water forms an important part in oil sand production: From steam required for heating bitumen for clay and sand separation to steam needed for bitumen processing and electricity generation. Canadian oil sand industry is striving to maximize recycling of water usage as well as finding alternative for fresh water. According to reports by CAPP about 80-95% of water used is recycled.

1.2. Motivation

Depletion of light petroleum has made the petroleum refining industry to explore opportunities in heavy or extra heavy oil. Heavy crude oils have low yield of lighter fractions and high yield of bottom residue. Hence in future the refineries would face a challenging task to upgrade the heavy oil to meet market requirements. Albertan oil sand bitumen has 15% by weight asphaltenes content. Asphaltenes are the heaviest fraction of solubility class with relatively high heteroatom and inorganic matter content. Processing and removal of asphaltenes would improve the time required to distill the crude oil[5]. Separation of asphaltenes from Cold Lake bitumen increased the degree API of the deasphalted oil (DAO). Improvement in degree API suggested that crude became lighter and rich in paraffins The hydrogen content of the oil increases and overall heteroatoms like sulfur, nitrogen decreases [6].

Upgrading of heavy oil or heavy bottoms assists the refiners in producing light, high value crude and valuable transportation fuels. Solvent deasphalting (SDA) and residue coking are most prevalent methods used by refiners for upgrading. One of the disadvantages of this type of upgrading is finding beneficial use for the by-products formed from these processes. Hence application of solvent deasphalting unit coupled with other processes like gasification and hydrotreating can lead to advantageous results [7].

Heavy residues from distillation column or SDA unit require further processing to be blended with valuable products and sold in market. Even so they are sold at repressed value. An integrated gasification, hydrocracking and power generation

can facilitate the operating flexibility of the refinery[8]. Heavy residues are converted into high value product (H_2, power) and other intermediate products such as DAO. DAO can undergo hydrotreating to produce valuable diesel. DAO can also be blended with vacuum gas oil to meet resid catalytic cracking feedstock specifications[7]. On gasifying the low value asphaltenes the refiners produce high value syngas (CO, H_2). The syngas gas can be converted into hydrogen which is further used in hydrotreating and hydrocracking units to obtain lighter fractions such as kerosene, gas oil. SDA requires significant amount of heat to separate solvent from the oil and asphaltenes such that it can be reused over period of time. Gasification helps in providing the necessary heat for solvent recovery. Syngas is also the precursor of numerous chemicals and can used as fuel in power generation. Integration of deasphalter and gasification units helps in minimising the NO_x and CO_2 emitted. Sulfur content in asphaltenes is quite high and SO_x formation occurs when distillates blended with asphaltenes is combusted. However, on asphaltenes gasification sulfur is converted to hydrogen sulfide which can be converted to elemental sulfur after removal from syngas.

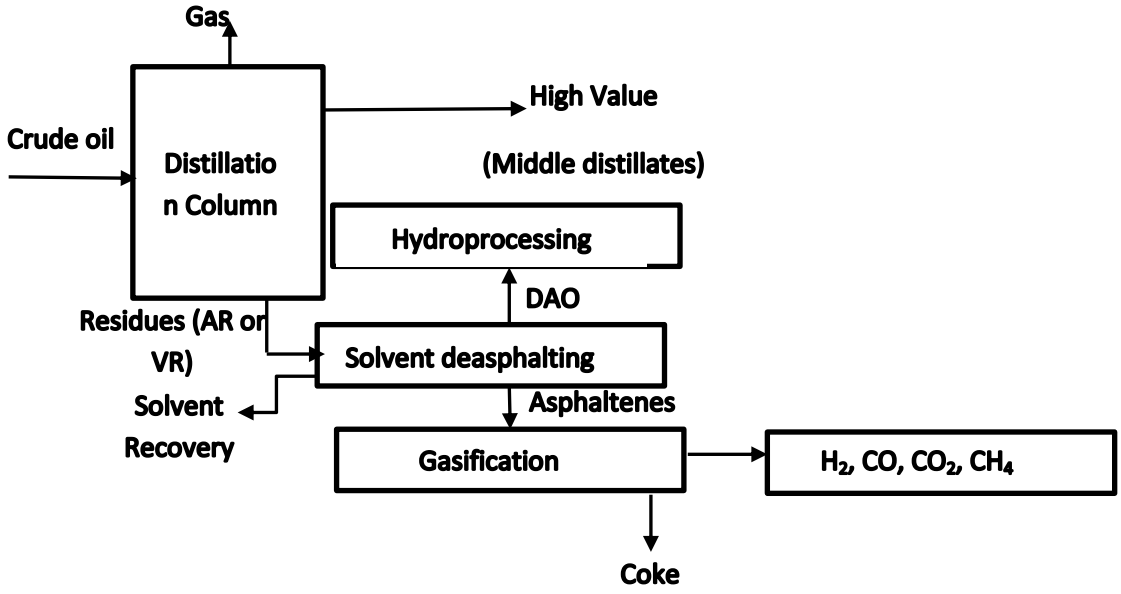

Figure 1.2: Integrated deasphalting and gasification scheme

Integration of SDA unit and gasification unit is utilized in Long Lake project Alberta, Canada. It is a joint venture between Nexen and OPTI Canada where 72,000 *bbl. /d(barrels per day)* of extracted bitumen undergoes upgrading into premium quality crude. Asphaltenes by-product from SDA is fed into the 3,600 *t/d (tons per day)* Shell gasification unit to generate hydrogen for hydrocracker process. Excess of syngas is used to generate steam that helps in bitumen extraction and improving its viscosity for pumping ability [9].

With limited work on gasification of asphaltenes, this study was initiated to get better understanding on influence of various parameters on the rate of gasification or intermediate pyrolysis step.

1.3. Gasification Overview

A good understanding of fundamental reactions is necessary to design, operate and troubleshoot a gasifier. Gasification is defined as conversion of any solid or liquid feed into useful gaseous fuel or chemical feedstock that can be burned to generate energy or produce valuable chemicals. Gasification and combustion are thermal processes, however they have prominent differences between them. Gaseous products formed from gasification have high energy value. Hydrogen is added to the feedstock during gasification process to give a higher H/C ratio while combustion oxidizes the carbon and hydrogen in feed to CO_2 and H_2O. A typical gasification process is shown in the Figure 1.3 below:

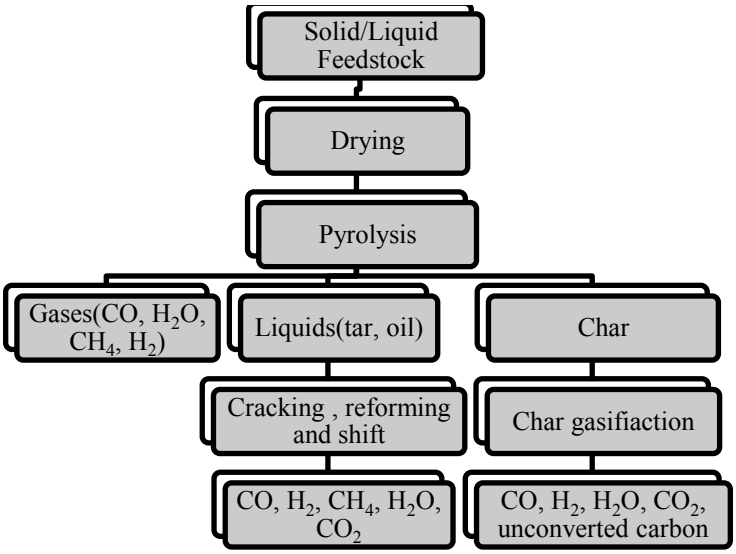

Figure 1.3: Path followed in gasification

Broadly, the gasification can be divided into following steps: Preheating/drying, Pyrolysis, Combustion and Char gasification. In most cases these step overlap on one another. Pyrolysis is the first step of all thermochemical reactions Large hydrocarbon molecules are broken down above 350˚C to produce hydrogen rich volatile products, tar, and gases. In case of fast pyrolysis more liquid hydrocarbon is expected while in slow pyrolysis more char is formed. The char formed during pyrolysis reacts with gasifying agents like steam, carbon dioxide, oxygen and hydrogen to give higher value products. The energy for endothermic reactions like pyrolysis and drying is provided by exothermic gasification reactions. The char-gas reactions are illustrated as below [10][11]:

Carbon Reactions

R1 (Boudouard)	$C + CO_2 \leftrightarrow 2CO$	$\Delta H = 172$ kJ/mol
R2(Water-gas or Steam)	$C + H_2O \leftrightarrow CO+H_2$	$\Delta H = 131$ kJ/mol
R3 (Hydrogasification)	$C + H_2 \leftrightarrow CH_4$	$\Delta H = -74.8$ kJ/mol
R4	$C +0.5O_2 \rightarrow CO$	$\Delta H = -111$ kJ/mol

Oxidation Reactions

R5	$C + O_2 \rightarrow CO_2$	$\Delta H = -394$ kJ/mol

R6	$CO + 0.5O_2 \rightarrow CO_2$	ΔH = -284 kJ/mol
R7	$CH_4 + 2O_2 \leftrightarrow CO_2 + 2H_2O$	ΔH = -803 kJ/mol
R8	$H_2 + 0.5O_2 \rightarrow H_2O$	ΔH = -242 kJ/mol
Shift Reaction		
R9	$CO + H_2O \leftrightarrow CO_2 + H_2$	ΔH = -41.2 kJ/mol
Methanation Reactions		
R10	$2CO + 2H_2 \rightarrow CH_4 + CO$	ΔH = -247 kJ/mol
R11	$CO + 3H_2 \leftrightarrow CH_4 + H_2O$	ΔH = -206kJ/mol
R14	$CO_2 + 4H_2 \rightarrow CH_4 + 2H_2O$	ΔH = -165 kJ/mol
Steam-Reforming		
R12	$CH_4 + H_2O \leftrightarrow CO + 3H_2$	ΔH = 206 kJ/mol
R13	$CH_4 + 0.5O_2 \rightarrow CO + 2H_2$	ΔH = -36 kJ/mol

Under similar conditions, combustion reactions are faster than gasification reactions with combustion reaction rate at least one order magnitude faster. The char- steam reaction is three to five orders slower than combustion reactions. Char – carbon dioxide reaction is six to seven order slow while steam gasification is faster than the Boudouard reaction [12]. Methanation reaction is slowest of all char –gas reactions occurring in a gasifier. The char particle temperature remains same as bed temperature in a gasifier because of endothermic and exothermic reactions occurring simultaneously [13]. Optimum amount of oxidant or steam is needed to maintain gasifier temperature as well prevent dilution of gaseous products by addition of excess CO_2.

1.3.1 Gasification Technology

Gasifiers can be categorised into *Moving bed reactor*, *Fluidized bed reactor* and *Entrained bed reactor* based on the flow of gasifying agent and feed.

A moving bed reactor can be further classified into *updraft gasifier* and *downdraft gasifier*. In an updraft gasifier fuel is fed from the top. The preheated gasifying agents like air, steam and oxygen enters the gasifier from bottom. The product

gases formed rise through the descending fuel or ash and leave from top. The bottom layer of the gasifier is the combustion zone where the temperature exceeds the ignition temperature of carbon. Highly exothermic reactions take place in the gasifier and the combustion reactions rapidly consume the oxygen present. Thus the combustion reaction changes into partial oxidation releasing CO. The mixture of CO, CO_2 and steam moves up into the gasification zone to gasify the upcoming char. Once the oxygen is completely depleted, the CO_2 formed enters into the gasification reaction leading to formation of CO. Such reactions are endothermic in nature and energy required for reactions is provided by the sensible heat from the gas. The reaction regions are different in case of downdraft gasifiers. Steam and air/oxygen is fed into the lower section of the gasifier along with the feed while pyrolysis and combustion product also flow downward. Such kind of arrangement results in tar free gases.

In fluidized reactor the fuel is fed from top or sides with the gasifying medium serving as fluidizing gas. Solid fuels are brought into contact with hot bed particles such as sand so that they quickly heat the feed to bed temperature releasing char, gases and tars. The fluidising gas remains in plug flow: enters from bottom and leaves at top. The oxygen undergoes fast exothermic reactions at the bottom of the bed with char formed during pyrolysis. The bed medium helps in distribution of the heat released by the exothermic reactions. Subsequently gasification reaction occurs as the gases rise up. A bubbling fluidized bed cannot achieve complete char conversion as they allow gas to bypass the solids without participating in any reactions. Fluidized bed gasifiers operate at low temperature range 800-1000°C to prevent agglomeration of ash. Hence most high ash fuels can be gasified without the problem of sintering. Biomass, lignite and municipal waste are preferred fuel in such kind of reactors [11].

Entrained bed gasifiers operate at high temperature 1400°C and pressure 20-70*bar* pressure and are most preferred in IGCC (integrated gasification combined cycle)

plants. Due to shorter residence time, the feed is in powdered form to enhance char gas reactions and sufficient gas velocity is maintained to fully entrain the feed particles. These types of gasifiers have feeding provisions both from top and sides. Feed in form of slurry can also be provided to the gasifier. Oxygen upon entering the gasifier undergoes rapid exothermic reactions resulting in rise of bed temperature above the melting point of ash. This result in high carbon conversion and complete destruction of tar formed during pyrolysis.

1.4. Thesis Outline

This thesis has been organised into 5 chapters for ease in understanding. The first chapter introduces the idea about Oil sands, its occurrence, production and impact on economy development of Canada. This chapter also covers the fundamentals of gasification technology along with motivation and objectives of current work.

The second chapter elaborates the importance of asphaltenes from various crudes, its structure and molecular weight, elemental composition and characterization techniques. Pyrolysis background and work done by researchers on fuels like coal, biomass and bitumen/asphaltenes has been discussed. Pyrolysis mechanisms and impact on char structure and morphology has also been reviewed. Few works related to single particle gasification and partial oxidation has been taken up due to relevance for current work. Finally, numerous methods for solid kinetics has been discussed with maximum focus on iso-conversional techniques for kinetic parameters calculation.

Details of experimental setup design have been chronicled in chapter 3. Apart from that, chapter 3 features feed and char preparation, details behind all the characterization techniques and those needed for partial oxidation and kinetic experiments.

Chapter 4 communicates all the results obtained from pyrolysis and partial oxidation experiments. Extensive study on char morphology and structure and its dependence on pyrolysis condition and particle size have been executed.

Importance of mineral matter and behavior during pyrolysis has also been recounted. Subsequently all work on oxidation, combustion reactivity, morphological changes in asphaltenes chars have been analyzed.

Chapter 5 concludes the major findings in present thesis work along with suggestion for possible research in future. Working of the drop tube furnace, calibration, estimation of particle temperature and repeatability of experiments has been appended in the Appendix.

1.5. Objectives

Effect of parameters such as particle size, furnace temperature, and heating medium are pronounced when work is carried on single particle behavior as they are conducted in controlled environment with elimination of complexities arising from particle interactions. Investigation of single asphaltenes behavior during pyrolysis and partial oxidation is the major objective of this work. The first segment of work necessitated design of lab-scale drop tube furnace so as to carry out entrained bed conditions. This fundamental study on single particles supplements the previous work on asphaltenes pyrolysis in drop tube furnace. The following objectives are aimed for the given study:

- To design lab-scale drop tube furnace for pyrolysis experiments
- To gain better understanding of operating parameters on: morphological and structural changes and inorganic matter retention behavior in char formed during pyrolysis
- To compare the morphology of char formed at varying partial oxygen pressure
- To investigate the combustion reactivity of char formed during pyrolysis

Chapter 2
LITERATURE REVIEW

2.1. Asphaltenes

According to Merdrignac and Espinat, heavy fractions of crude oil have 25 or more carbon atoms uniformly distributed in resins and asphaltenes[14]. Asphaltenes are harbinger of sediments and sludge in pipelines across refinery industries. As a result of high metal content asphaltenes deposit on catalyst in fluid catalytic units and cause deactivation by blocking the active sites [15]. Amount of saturates and aromatic content depends on the nature of crude. Highly aromatic asphaltenes in crudes renders it unstable and can lead to precipitation. This is attributed to the ease of separation of aromatic asphaltenes from the alkane/paraffinic rich phase [16]. Various researchers have different definition for asphaltenes. According to Demirbas, asphaltenes is constituted of aromatic rings with alkyl bridges of 30 carbon atoms, ketones, phenols and carboxylic acids. Heteroatoms like nitrogen is present in pyrrole and pyridine form while sulfur is prevalent as benzothiopene rings. Transition metals like nickel and vanadium are present in complex porphyrinic structure with nitrogen [17]. Most widely used definition is based on terms of solubility class. Asphaltenes are the fraction in crude which remain insoluble in alkanes like n-pentane, n-heptane but soluble in aromatics solvents like toluene. Lighter paraffin like n-pentane have the ability to precipitate more compared to n-heptane because they separate resins along with asphaltenes. Upto 30*wt.*% of material is precipitated when n-pentane is used [18]. n-heptane has an advantage of retaining the properties of asphaltenes during precipitation [19]. However , n-heptane yields low amount of asphaltenes ,about 15-98% less than n-pentane depending of type of crude [20]. Precipitation of asphaltenes improves the hydrogen content of the other fraction along with significant decrease in sulfur, nitrogen and oxygen.

2.1.1. Asphaltenes Structure and Molecular Weight

Calemma et al with the help of nuclear magnetic resonance(NMR), electron paramagnetic resonance(EPR) and Fourier transform infrared(FTIR) deduced that asphaltenes molecule could be represented in terms of polycondensed groups with 5-7 aromatic rings bridged by aliphatic chains and heteroatoms [21] .This hypothetical molecular structure of asphaltenes had more aromaticity with decrease in length of alkyl side chains. This fact is also corroborated by Mullins with help of fluorescence depolarization [22][23]. Speight and Moschopedis predicted the empirical formula for asphaltenes to be $C_{80}H_{80}N_2S_2O$ with molecular weight of 1,150*g/mol* bearing aliphatic chains on core of aromatics [24]. However with the advent of techniques on mass spectrometry like fluorescence depolarization the complex structure of asphaltenes has become passé. According to Groenzin and Mullins, the variety of asphaltenes are huge with asphaltenes molecule being covalently attached to structures such as thiophene, porphyrins, sulfide, pyrrole, pyridine, aromatics and simpler alkyl chains [23].

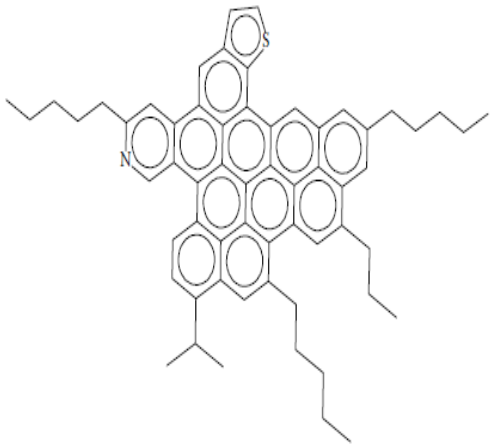

Figure 2.1: Hypothetical structure of asphaltenes [24]

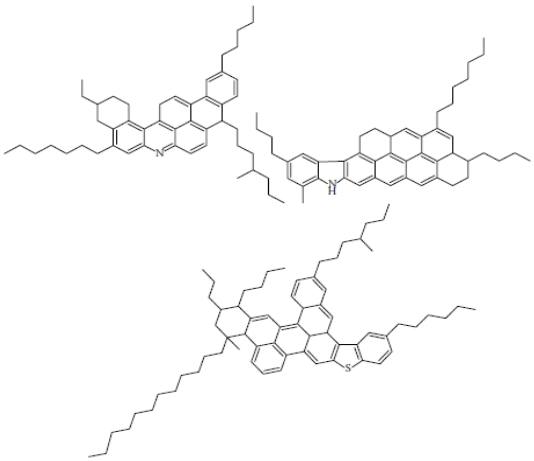

Figure 2.2: Ideal molecular structure of asphaltenes consistent with rings and composition [23]

Molecular model and simulations also helped in chemical characterization of asphaltenes structure. Aguilera et al proposed that asphaltenes structure can be modeled into two categories: *continental type* where asphaltenes have fused aromatic cores with more than seven rings and *archipelago type* where asphaltenes with small aromatic cores are linked to one another by bridging alkyl chains [25]. Zhao et al using fractionation method for extraction of various cuts in residual oils proposed that asphaltenes are composed of pericondensed polyaromatic rings, hence validating the continental type of structure [26]. Substantial work has been done on stable and unstable asphaltenes from Venezuelan crude oils. Stable asphaltenes have lower molecular weight of 1,000 *g/mol* while unstable ones have higher weight of 1,200*g/mol* due to significant presence of heteroatoms [27]. Small angle neutron technique along with pyrolysis and thermal degradation has supported the archipelago structure of asphaltenes[28]. Speight has suggested more heteroatomic nature of asphaltenes ($C_{116}H_{133}NOS_3$) with molecular weight of 1,653*g/mol* in archipelago style [29]. Quantitative data from Monte Carlo simulation indicated archipelago type of structure possessing small aromatic rings linked by sulfur and alkyl bonds [30]. Depending upon the type of structure the asphaltenes rearrange themselves in a solution. The archipelago type tend to stack themselves in a column while continental type have

the propensity to form planar structure [31]. Few researchers employed techniques like Scanning Tunneling Microscopy and Fluorescence Emission Spectroscopy to estimate the number of aromatic rings in asphaltenes molecule. They stated that asphaltenes consist of 4 to 10 rings with diameter of the aromatic core around 11-14$\mathring{A}$ [32][33][34]. Asphaltenes have more pericondensed structure than the corresponding resins. The force balance between steric hindrance by alkyl chains and Van der Waals interactions through π bonds determines which fractions fall into asphaltenes category. Absence of alkyl hindrance might reduce the solubility of aromatic rings [35].

2.1.2. Asphaltenes Density

Weight fraction of asphaltenes(w_{asph}) in heavy oil can be used to obtain the density of asphaltenes through following equation [36]:

$$\rho_{asph} = \frac{w_{asph}}{\frac{1}{\rho_{oil}} - \frac{1 - w_{asph}}{\rho_{maltene}}} \tag{2.1}$$

The density of asphaltenes from Lloydminster area in Canada is estimated to be 1,175 kg/m^3 through above relation. Molecular weight (MW), carbon number(C_n) and aromaticity of the fraction(f_a) are used to determine the specific gravity of the cut fraction [37].

$$SG = 0.846e^{(0.6807 f_{ar})} + 0.0003C_n - \frac{1}{0.72C_n e^{(-3.26 f_{ar})} + 1.2} \tag{2.2}$$

The carbon number is approximated from work of Whitson [38]:

$$C_n = \frac{1}{14}(MW + 6) \tag{2.3}$$

f_{ar} and C_n obtained by ^{13}C NMR experiments are specific for asphaltenes obtained from different regions [37]:

For Athabasca bitumen:

$$f_{ar} = -0.0717 Ln(C_n) + 0.73 \tag{2.4}$$

For Cold Lake bitumen:

$$f_{ar} = -0.0647Ln(C_n) + 0.73 \quad (2.5)$$

Yarranton and Masliyah carried experiments to find correlation density of asphaltenes and insoluble fractions precipitated from toluene solutions. The plot between reciprocal mixture density(ρ_M) and asphaltenes mass fraction(x_A) can assist in density calculation [39].

$$\frac{1}{\rho_M} = \frac{1}{\rho_T} + (\frac{1}{\rho_A} - \frac{1}{\rho_T})x_A \quad (2.6)$$

Athabasca asphaltenes have a density of 1,162kg/m^3 based on the approximation and assumption of above correlation.

2.1.3. Variables affecting Asphaltenes Precipitation

Asphaltenes precipitation is influenced by various parameters such as medium of containment, nature of parent crude, contact time, temperature, pressure and solvent to crude ratio [40]. Addition of paraffinic solvents disrupts the asphaltenes-resin equilibrium leading to increase in concentration of asphaltenes monomer. After a critical content , asphaltenes separation occurs from the bulk phase [41]. With impact of weather conditions, the composition of crude oils changes with location and depth of mining. Elemental composition such as Vanadium content is a major variant in such cases. Past work has shown a possible correlation of asphaltenes content with vanadium [42]. Increase in vanadium content reduces the degree API gravity indicating a good proportion of asphaltenes. Solvent with good dissolving properties enhances the aggregation power of asphaltenes resulting in high molecular weight of the precipitate. Speight et al established that iso-paraffins have better solubility strength than terminal olefins. However aromatics are best for dissolving asphaltenes [43]. Among paraffins, n-heptane give constant amount of asphaltenes with better repeatability of experiments [44]. With increase in carbon number the amount of asphaltenes precipitated decreases but they become heavier with high polarity [45][46]. Solvent to oil ratio for asphaltenes

precipitation is kept at 40:1 for n-pentane while it is 60:1 for higher paraffins and iso- paraffins [24][47]. Contact time for solvent and asphaltenes mixing is crucial in amount of asphaltenes precipitated. Standard procedures suggest 15*min*-1*hr* contact time when n-heptane is used as solvent. Modified ASTM method recommends contact times of 8*hr* for constant amount of asphaltenes precipitation[48]. Asphaltenes precipitation decreases with temperature rise when solvents like n-pentane, n-heptane, n-decane and n-dodecane are used [45][46][49] . This can be credited to the fact that with increase in temperature, asphaltenes solubility in crude oil increases hence retarding the precipitation process. But increase in precipitation temperature leads to precipitation of porphyrinic compounds of Ni and V [50].

2.1.4. Elemental Composition of Asphaltenes

Speight and León suggested that unstable crude are dearth in hydrogen content indicating greater aromaticity with condensed rings [24][51]. Precipitation with n-pentane leads to high H/C atomic ratios while n-heptane precipitation gives more oxygen, nitrogen and sulfur content. Increasing API gravity of crudes reported linear increase in Ni and V content [52].

Organic nitrogen in asphaltenes has adverse effect on catalyst and product cause deactivation and instability respectively. Basic nitrogen structures such as quinolone and acridine are strong inhibitors of Hydrotreating (HDT) reactions than normal carbazole and indole structures. Asphaltenes contains nitrogen in aromatic forms with small amount of saturated amines such that pyrrole form is prevalent than pyridine structure [53]. Additional structures such as carbazole, methyl, dimethyl and benzocarbazoles have also been identified by gas chromatography [54][55]. Low molecular mass asphaltenes has nitrogen in form of benzocarbazoles and substituted carbazoles. Nitrogen can attach themselves to transitional elements and exist in form of vanadyl porphyrins with 22-52 carbon atoms [20]. Ion exchange chromatographic fractionation of Athabasca bitumen indicated presence of 39.8 *wt.* % acids, 23.3 *wt.* % basics, 20.2 *wt.* % neutrals and

16.9 *wt.* % amphoterics. Acid nature is predominant due to high oxygen content than nitrogen and sulfur. Acidity is due to compounds such as carboxylic acids, benzoic acids, phenol, indole and carbazole while basicity is related to pyridine, pyrazine, dimethylformamide and dimethylsulfoxide [56][57].

Mullins and Kelemen stated that sulfur in asphaltenes is present in thiophenic form , mostly benzo and dibenzothiophenes [58][59][60]. Sulfur content is higher than respective maltenes and can range from 6-8 *wt.* %. Athabasca asphaltenes might have acylic sulfur linkages.

Oxygen present in asphaltenes has been identified as carboxylic, phenolic and ketonic forms. Oxygen in the form of ester and ether bonds are bonded by C-O and C-C bonds to asphaltenes structure [61][62]. Low molecular weight Athabasca asphaltenes characterization illustrated presence of oxygen as fluorenones , substituted fluorenones , penta-cyclic terpenoid carboxylic acid, carboxylic acids of dibenzothiophenes and bi-,tri-, penta-cyclic terpenoid sulfoxides [63].

2.1.5. Asphaltenes Characterization

Due to complex nature of asphaltenes more sophisticated instruments are required for characterization of asphaltenes. Few popular methods involve Infrared spectroscopy, vapor pressure osmometry and mass spectroscopy. GC-MS provides incomplete characterisation with only 74 w*t.*% of the sample analyzed[18]. Infrared spectra of asphaltenes show characteristic symmetric stretching of C-H aromatics and C-H aliphatics at 3,057cm^{-1} and 2,922cm^{-1} respectively. Aromatic bending is prominent at 870cm^{-1} while methyl groups did the same at 722cm^{-1}. Alkene C=C stretching is significant with vibration from 1,609-1,580cm^{-1}. Sulfur in form of thioether or with any -C-S-C- structure have vibration around 2,500cm^{-1} [35]. FT-IR spectra helps is providing additional information on the quantity of asphaltenes in crude oils [64].

Asphaltenes molecular weight has always been an enigma for researchers. Based on separation methods or colligative properties different techniques provide a

wide range of molecular weight. One of the popular techniques is Vapor pressure osmometry (VPO). VPO gives robust results for low molecular weight and non-polar compounds by providing absolute value instead of number average weight. For Athabasca and Cold Lake asphaltenes VPO gives value from 4,000-10,000 *g/mol* [65]. Asphaltenes are the small fraction of bitumen obtained but has highest molecular weight with aromatics and saturates having same molecular weight. Size exclusion chromatography (SEC) is another frequently used technique to obtain reliable distributions of molecular weight with proper solvent choice for separation.

Internal structure of asphaltenes can be characterized by XRD techniques just like coals. XRD analysis provides relevant information on aromatic stacking and possible crystallites formation. Spacing between the aromatic layers has resemblance to that of graphene band. However, on heating the asphaltenes sample these graphene like bands tend to disappear.

2.1.6. Significance of Asphaltenes

Asphaltenes is thought to be an aspect in petroleum operations such as transportation, refining, wax crystallisation and emulsification/de-emulsification. Changes in temperature, pressure or composition of crude oil leads to precipitation and deposition of asphaltenes during production and transportation through pipelines. Precipitation can cause reduction in permeability of the reservoir resulting in plunging of tubing and wellbore. During processing asphaltenes can deposit on the catalyst or accumulate gradually on equipment causing reduction in efficiency and operational hazards.

Apart from being abominable, asphaltenes are crucial in revealing reservoir fluid history and characteristics. They affect fluid viscosity, density and stabilise oil-water emulsion [5].

2.2. Pyrolysis of Asphaltenes and other Fuels

Pyrolysis is the first stage of all thermochemical decomposition in any organic material at high temperature in an inert atmosphere. Application of pyrolysis dates back to ancient Egyptian civilization where people obtained methanol from wood pyrolysis for embalming process. Pyrolysis accompanies complex changes in morphology and reactivity of chars which can in turn affect the subsequent gasification stage. Complicated pyrolysis reactions involve bond breaking, vaporization, crosslinking and condensation of various aliphatic and aromatic groups. In coals most pyrolysis reactions commence at 397°C by overcoming the C-C bond energy [66]. The bridges is ring structures of fuel are first to break and form free radicals. These reactive free radicals readily combine in the gas phase to produce lighter hydrocarbons such as methane. Typical reactions taking place with temperature increase has been illustrated below [66]:

Cracking:	$R\text{-}CH\text{-}R' \rightarrow R\text{-}R' + \text{-}C\dot{H}_2$
Saturation:	$\text{-}C\dot{H}_2 + 2H' \rightarrow CH_4$
	$\text{-}OH + H' \rightarrow H_2O$
Tar formation:	$\text{-}R\text{-}CH_2 + H' \rightarrow R\text{-}CH_3$
Crosslinking/Condensation:	$R\text{-}OH + H\text{-}R \rightarrow R\text{-}R + H_2O$
	$R\text{-}H + H\text{-}R' \rightarrow R\text{-}R'$ (coke/char) $+ H_2$

Release of CO_2, H_2O and CH_4 components during pyrolysis exalts crosslinking reactions. Depletion of H_2 from aliphatic and aromatic portion of the fuel culminates the primary pyrolysis. Secondary pyrolysis involves removal of additional gas such as HCN from nitrogen containing ring components, CO from ether links, CH_4 from methyl groups and finally H_2 from ring condensation.

Further pyrolysis reactions can be classified as *slow* and *fast* pyrolysis. High heating and heat transfer rates, short residence times and high yields of liquid at controlled temperatures are few essential features of fast pyrolysis processes [67]. Substantial work has been done on effect of particle size, wall temperature,

heating conditions on pyrolysis of coal samples. Large coal particles refrain movement of volatile matter and aid secondary reactions leading to increase in lighter gases and decrease in tar yield [68]. Coal devolatilization comprises another influential factor: char structure. The ultimate structure of char is determined by behaviour of volatile release rather than actual feed pore structure. This gave rise to multi bubble mechanism which indicated that volatile matter is transported in the form of bubbles through the soft phase during pyrolysis. With existence of large number of bubbles the volatiles diffuse from one bubble into another resulting in swelling of coal particle. Finally on reaching the surface of particle the forces are overcome and volatile matter is released [69]. The char structure formed plays significant role during char gasification. Presence and distribution of pores on char determine the diffusion of reactant gases on char surface which is rate limiting step. Extensive loss of volatiles results in highly porous chars and such char are expected to have early burnout during combustion. Macropores(pore diameter $>5\mu m$) and mesopores($0.2nm <$ pore diameter $< 5\mu m$) have marked effects on char reactivities during CO_2 gasification [70]. Whereas others chose to differ by suggesting good correlation between char micropores(pore diameter $< 0.2nm$) and reactivity [71]. Porous chars have higher chances of fragmentation and enhanced gasification rates [72]. Fragmentation affects the particle size distribution of final ash with increased generation of finer ash [73]. The char structures are classified as: Group A cenospheres with thin wall balloon shaped, Group B cenospheres with thick wall and Group C cenospheres with ribs (honeycomb structure) [73]. As the furnace temperature increases coals produce thin walled chars with larger central pores and voids.

In early 1984, Behar et al studied the characterization of various asphaltenes by pyrolysis chromatographic technique. Pyrolysis yields at 550°C confirm the preconceived structures of asphaltenes: *pericondensed asphaltenes*, *kata-condensed asphaltenes.* The products of asphaltenes pyrolysis have n-alkanes distribution in ranges upto C_{30}.They also concluded that hydrocarbons and

asphaltenes of oil shared common origin based on the distribution of n alkanes[74]. Further studies on asphaltenes pyrolysis are carried out using batch reactors. Trauth et al isolated the maltenes, asphaltenes and coke product from pyrolysis experiments of Hondo and Maya vacuum resids using solvent extraction method. The kinetic pathways suggested that isolated asphaltenes are more reactive that asphaltenes in resid. The apparent activation energy of Hondo asphaltenes in resids fraction as well as isolated case is lower than their counterpart Maya resids. Gas chromatography indicated similar evolution in both the resids pyrolysis but Hondo asphaltenes gave higher H_2S evolution [75]. Characterization of Mayan asphaltenes indicates paraffins in range C_7-C_{20}, cyclo-paraffins, aromatics in form of mono/penta aromatics or thiophene aromatics and finally polar fractions as esters, ketones, alcohols, amides and acids [76]. Zhao et al investigated the carbonization in pyrolysis of asphaltenes derived from Athabasca bitumen. They reported that coke and gas yield increases as the temperature of the bath reactor increases from 430-550°C but there is decrease in liquid yield. According to their observation the carbonization follows complex mechanisms involving cyclization of alkyl chains, dehydrogenation, aromatization ,condensation and peri-condensation of aromatic rings [77].

2.3. Previous Works on Single Particle Investigation

Single Particle investigation is a realistic and well defined method for any fundamental studies. Effects of variation in parameters such as composition, ash and moisture content, particle size and temperature are suitable for studies in such investigation. Analysis of single particle has been well applied to coal, biomass and heavy oil combustion and pyrolysis.

Ricky Chan et al pyrolyzed single and thermally thick lodgepole pinewood in a radiantly heated glass reactor. Gas sampling and temperature measurement is carried throughout the experiment. Wood anisotropy has effect on pyrolysis products such as tar and gas. This property favors char forming reactions with decrease in yield of tar and increase in production of gas and char. The heating

rates also have substantial effect on particle size and reactivity. At low heating rates, 0.5*cm* increase in particle size results in 28% decrease in reacted fraction while for high heating rates for similar condition there is 4-7% decrease only [78]. Moisture content also has pronounced effect on tar and char yield. An increase in moisture content (by 60% dry basis) leads to decrease in char yield by 15 % and increase in tar yield by 60%. In a recent work by Maryam Momeni, devolatilization , ignition and burnout behavior of single biomass particle is studied in a furnace by varying gas temperature and oxygen concentration in the range of 1200-1600°C and 5-20% respectively [79]. Oxygen concentration has a noticeable impact on ignition delays and devolatilization at lower furnace temperatures. Moreover heterogeneous ignition (due to hemicellulose and cellulose decomposition) is detected for all conditions followed by secondary homogenous ignition when large particles are considered for study.

In 1996, Moszkowicz studied the emission of solid particles mostly cenospheres during fast pyrolysis of heavy fuel in a boiler. The experiments constituted of feeding stream of single droplets of heavy fuel in a crystal glass tube maintained at 1000°C. Particle size is varied from 140μm to 200μm and the atmosphere is kept inert. Cenospheres formed are collected using a bag filter of mesh 40μm and analyzed under SEM. They observe that cenospheres formation ratio is independent of varying size, residence time and high boiler temperature. Cenospheres have same honeycomb morphology with diameters ranging between 50-600μm. High boiler temperature and lower particle gave complete pyrolysis with less coking. However there is accumulation of thin solids of the surface of cenospheres resulting in increase of diameter. Volatile combustion during initial stage of pyrolysis gives rise to cracking reactions. This intensifies the solids formation but are preamble to volatile release [80]. Combustion of oil droplets on a hot surface shows similar stages of heating as that of droplet freely translating in space. A high temperature of the plate boosts liberation of lighter hydrocarbons while high carbon containing components tend to polymerize or form coke [81].

Surface texture such as roughness and contact angle play crucial role at temperatures below 550°C whereas they have insignificant influence above 550°C.

According to Bartle et al asphaltenes content in heavy oil is responsible for soot particles and cenospheres presence in emission during combustion [82]. Droplets of heavy fuel with diameter range 300-2000μm is heated in an electrically heated drop tube furnace in presence of air. They suggest that the asphaltenes contained heavy fuel has more submicron soot and larger cenospheres formation than asphaltenes free fuel. Furthermore, surface area of cenospheres increases with asphaltenes content. However asphaltenes presence reduces the ignition delay time due to high low molecular volatiles formation during pyrolysis stage.

Current study by researchers from Tampere University of Technology focuses on the use of high speed digital camera in a vertical two stage drop tube furnace for vaporizing oil droplets. Droplet velocity measurements indicate that there is acceleration during the devolatilization in the hot zone. Droplet diameter change is inconsistent with the increasing furnace temperature. This is associated with incomplete vaporization at low furnace temperatures [83].

2.4. Work on Partial Oxidation in Entrained Conditions

Moghtaderi et al suggest that improper char burnout leads to formation of incomplete combustion products. Incomplete combustion is a forerunner of pollutant formations as well as it renders the ash unsuitable for further use[84].Premature extinction of char particles caused by unstable combustion or sintering effects is responsible for incomplete burnout. They observed that at a given gas temperature, the burnout decreases with reduction in biomass size [84]. With stringent global regulation on CO_2 emission several strategies have been employed for capture or reduction of CO_2 from large scale power plants. In conventional coal- air combustion, the concentration of CO_2 is low and storage is not economically attainable. To increase the concentration of CO_2 in flue gas (upto 95%), coal is combusted in presence of oxygen and recycled flue gas

containing primarily CO_2 and H_2O. Replacement of N_2 by CO_2 affects the operation of the furnace as there is decrease in gas temperature and increase in unburnt carbon content. Study by Rubeira et al suggests overcoming of this situation by increasing the O_2 concentration by 30-35% so as to get similar burnout as conventional coal-air combustion in boiler [85][86]. This difference in behavior is attributed to lower diffusivity of O_2 in CO_2 compared to diffusivity in N_2. Lower diffusivity affects the transport of O_2 onto the surface of particle thus leading to reduced char combustion [87][88]. The burnout during combustion is calculated from ash content of coal (A_{coal}) and char(A_{char}) samples and is determined from following equations [88][89]:

$$Burnout = 100 \times [\frac{1 - (A_{coal}/A_{char})}{1 - A_{coal}}] \quad (2.7)$$

$$Burnout = 100 \times [1 - \left(\frac{A_{coal}}{100 - A_{coal}}\right)\left(\frac{100 - A_{char}}{A_{char}}\right)] \quad (2.8)$$

2.5. Kinetic Parameters through Non-Isothermal Method

External factors such as heating rate, temperature, residence time, pressure, fragmentation and size of particles are pivotal in influencing the nature of complex pyrolysis reactions as well as char oxidation. It becomes necessary to understand the products of pyrolysis for process optimization. Similarly the combustion reactivity of chars formed at commencement of gasification in reactor can be a critical process parameter. For smaller size fraction and less reactive coal, combustion is kinetically controlled rather than diffusion limited [90]. Massive loss of active sites, drop in hydrogen content as well as progressive order of char structures with increased pyrolysis temperature is responsible for reduced combustion reactivity. Penetration of oxygen during combustion governs the advancement of pore structure and porosity in coal or any solid fuel. Slower reaction rate favors diffusion of oxygen into micropores as well as macropores

while a higher rate accesses the most favorable sites: macropores. Elevated temperature improves the dominance of macropores in coal [91]. Mineral matter in coal sample is also instrumental in influencing the reactivities. Activation energy calculated for chars obtained from demineralized coal lignite are higher than their parent coal indicating that chars are less reactive than coal lignite. Similar study is also applicable for chars obtained from asphaltenes pyrolysis.

Combustion and pyrolysis mechanism, kinetic parameters are investigated from thermogravimetric analysis (TGA) data. Of the various methods to analyze the available kinetic data, model fitting method and model free (Isoconversional) method are widely popular. Model fitting methods require appropriate choice of reaction models which is based on supplementary information such as morphological studies. Isoconversional method helps to forgo limitations faced by model fitting methods as they aid in estimation of apparent activation energies without the knowledge of a detailed model for the reaction path. They are based on the assumption that same products are produced irrespective of the heating rates in the TGA. Apparent activation energies are obtained at progressive degrees of conversion by conducting collective experiments at different heating rates in TGA. A schematic diagram can be represented to show various ways to obtain kinetic parameters. Model free methods also has its own limitations, hence a reaction model is necessary to complete the kinetic study.

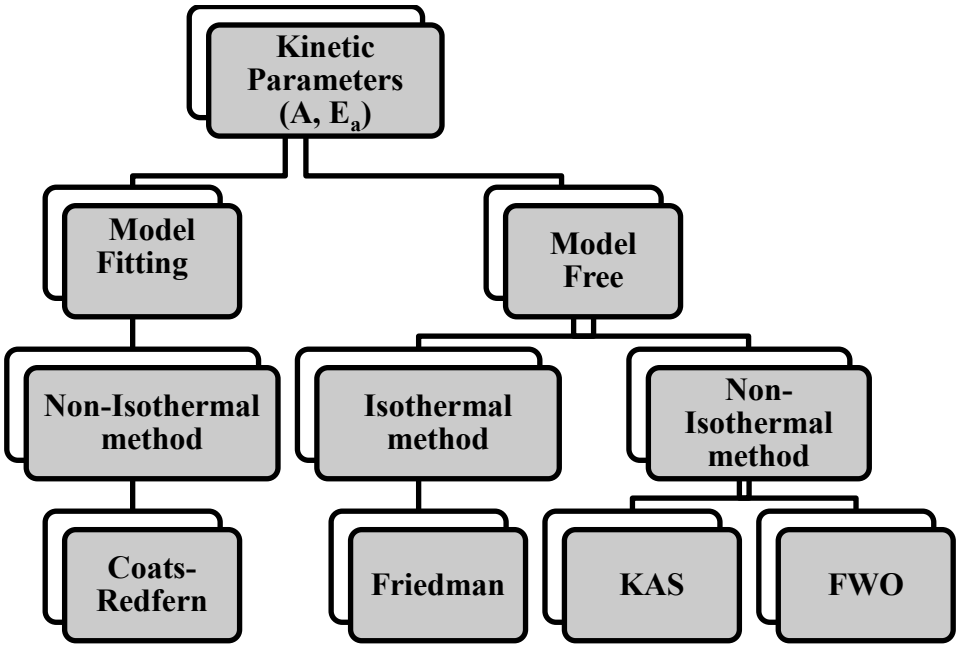

Figure 2.3: Methods for studying solid-state kinetics

The governing relation for kinetic analysis of any solid state decomposition (pyrolysis or combustion) can be expressed as:

$$\frac{d\alpha}{dt} = \beta \frac{d\alpha}{dT} = k(T)f(\alpha) \tag{2.9}$$

where α is the degree of conversion, t is the time taken, $k(T)$ represents the temperature based rate constant, $f(\alpha)$ is the reactions model and β is the heating rates from TGA experiments. The analytical forms of reaction models $f(\alpha)$ is readily available from literature [92]. The above equation can be further simplified in terms of activation energy (E_a) and frequency factor (A).

$$\frac{d\alpha}{dt} = \beta \frac{d\alpha}{dT} = \mathrm{A}e^{Ea/RT} f(\alpha) \tag{2.10}$$

Kissinger Akahira Sonuse (KAS) Method

The standard equation can be rewritten as:

$$\frac{d\alpha}{f(\alpha)} = \frac{A}{\beta} \exp\left(-\frac{E_a}{RT}\right) dT \tag{2.11}$$

which is integrated with initial conditions of α=0 at T=T_0 to obtain the expression:

$$g(\alpha) = \int_0^{\alpha} \frac{d\alpha}{f(\alpha)} = \frac{A}{\beta}\int_{T_0}^{T} \exp(\frac{-E_a}{RT})dT \quad (2.12)$$

This method assumes that A, E_a and $f(\alpha)$ are independent of final temperature and based on approximation the following relation is achieved.

$$ln\frac{\beta_i}{T_{\alpha i}^2} = ln\frac{A_\alpha R}{E_\alpha g(\alpha)} - \frac{E_\alpha}{RT_{\alpha i}} \quad (2.13)$$

The plot of ln β/T^2 vs 1/T at a constant value of conversion gives a straight line whose slope can be used to evaluate the apparent activation energy.

Flynn Wall Ozawa (FWO) Method

This method also follows the integral Isoconversional method.

$$ln\beta_i = ln\frac{A_\alpha E_\alpha}{Rg(\alpha)} - 5.331 - 1.052\frac{E_\alpha}{RT_{\alpha i}} \quad (2.14)$$

Coats-Redfern Method

Coats-Redfern method is also an integral method which uses an approximation $2RT/E_a<<1$ to obtain

$$ln\frac{g(\alpha)}{T^2} = ln\frac{AR}{\beta E_a} - \frac{E_a}{RT} \quad (2.15)$$

Coats-Redfern method helps in determining the most probable model for pyrolysis or combustion of asphaltenes and char obtained from devolatization respectively. The value for $g(\alpha)$ of various models has been illustrated in table below [93]:

Table 2.1: Solid state models and its g(α)

Mechanism	f(α)	g(α)
Power law(P2)	$2\alpha^{1/2}$	$\alpha^{1/2}$
Power law(P3)	$3\alpha^{2/3}$	$\alpha^{1/3}$
Power law(P4)	$4\alpha^{3/4}$	$\alpha^{1/4}$
Avarami-Erofe'ev(A2)	$2(1-\alpha)[-\ln(1-\alpha)]^{1/2}$	$[-\ln(1-\alpha)]^{1/2}$
Avarami-Erofe'ev(A3)	$3(1-\alpha)[-\ln(1-\alpha)]^{2/3}$	$[-\ln(1-\alpha)]^{1/3}$
Avarami-Erofe'ev(A4)	$4(1-\alpha)[-\ln(1-\alpha)]^{3/4}$	$[-\ln(1-\alpha)]^{1/4}$
Contracting area(R2)	$2(1-\alpha)^{1/2}$	$[1-(1-\alpha)^{1/2}]$
Contracting volume(R3)	$3(1-\alpha)^{2/3}$	$[1-(1-\alpha)^{1/3}]$
1D diffusion(D1)	$1/2\alpha$	α^2
2D diffusion(D2)	$[-\ln(1-\alpha)]^{-1}$	$[(1-\alpha)\ln(1-\alpha)]+\alpha$
3D diffusion(D3)	$3(1-\alpha)^{2/3}/[2(1-(1-\alpha)^{1/3})]$	$[1-(1-\alpha)^{1/3}]^2$
Ginstling Brounstein(D4)	$3/2((1-\alpha)^{-1/3}-1)$	$1-(2\alpha/3)-(1-\alpha)^{2/3}$
First order(F1)	$1-\alpha$	$-\ln(1-\alpha)$
Second order(F2)	$(1-\alpha)^2$	$(1-\alpha)^{-1}-1$
Third order(F3)	$(1-\alpha)^3$	$[(1-\alpha)^{-2}-1]/2$

Chapter 3
EXPERIMENTENTAL STUDY

3.1. Setup Design

The atmospheric entrained flow gasifier used for pyrolysis and partial oxidation studies is shown in Figure 3.1. The setup consists of small Thermolyne type 21100 furnaces. The overall furnace unit consists of a control unit, a tubular heating chamber and pyrometer. Heating chamber is 47*cm* long and 40*cm* wide. It consists of Al-Cr-Fe coil embedded in the rigid refractory material which is ceramically insulated. The temperature of the furnace is controlled by an input controller which compensates for fluctuations in line voltage and ambient temperature change. The temperature is measured by K-type thermocouple and registered in a pyrometer. All the electrical connections are housed in the control unit located below the furnace. The maximum working temperature is 1093°C when used intermittently and 982°C for continuous use (more than 3 *hrs*). The furnace is used to heat a quartz tube of length 60*cm* and inner diameter of 5*cm*. The exposed parts of quartz tube is insulated by K-wool and Aluminum-Silica Fiberfrax material to prevent any heat loss A double valve feeder as shown in Figure 3.2, is used to feed asphaltenes particle one at a time. A primary flow of N_2 is used in pyrolysis experiments to entrain the feed particles. Gas flow rates are adjusted using Cole-Parmer flow meters. The top part of quartz tube is closed by a flange with two ports: one for feeding and other for gas flow. The lower part of the tube has a quarter inch outlet for removal of volatiles formed. Volatiles formed during the experiments move to activated carbon filter for removal of heavy tar as well as particulate matters. Then it is further passed into water scrubber for removal of acid gases such as H_2S. Rocker 300 series pump is used at the end of scrubbing flask in order to maintain a unidirectional flow of volatiles. It also helps in controlling the pressure inside the quartz tube at 1*atm*. A 45° degree inclined mirror is placed at the bottom of the quartz tube to view the reaction occurring inside. The schematic representation could be seen in Figure 3.3.

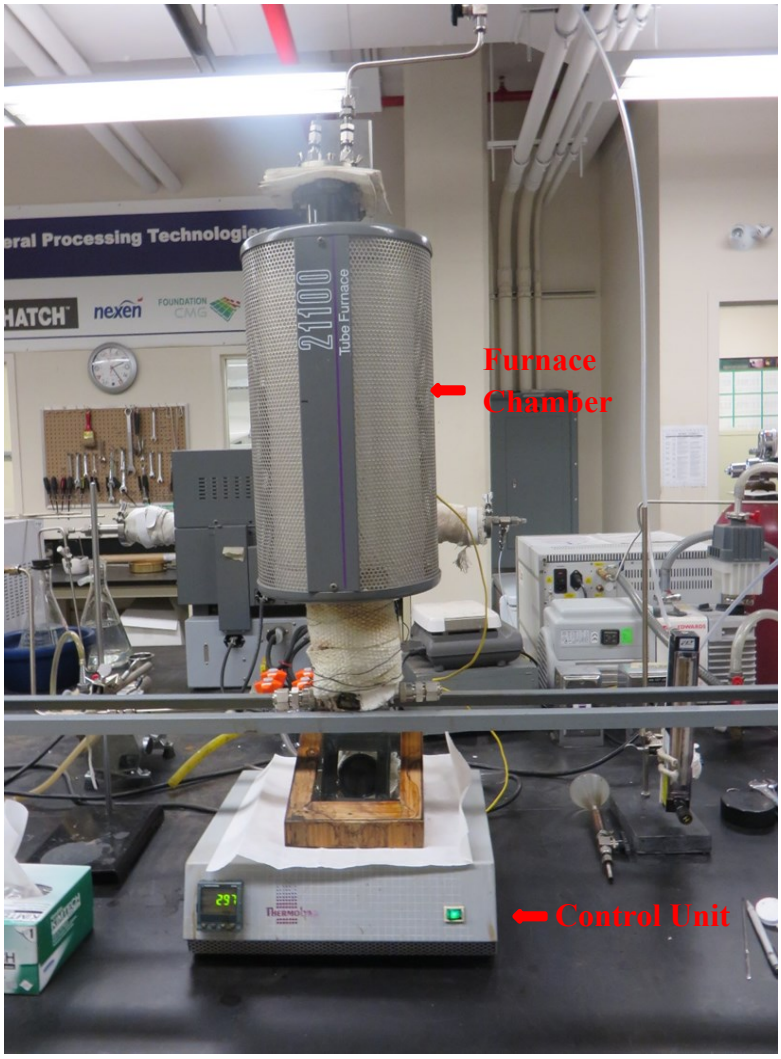

Figure 3.1: Vertical tube furnace used for pyrolysis and partial oxidation

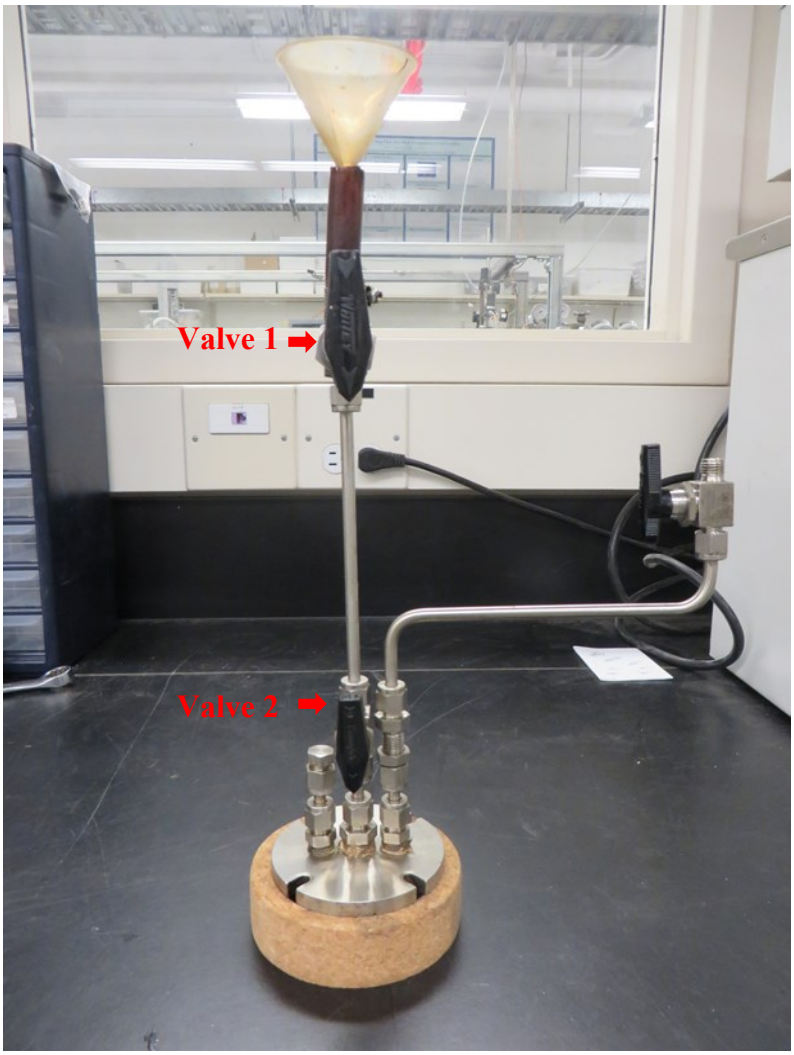

Figure 3.2: Double valve feeder

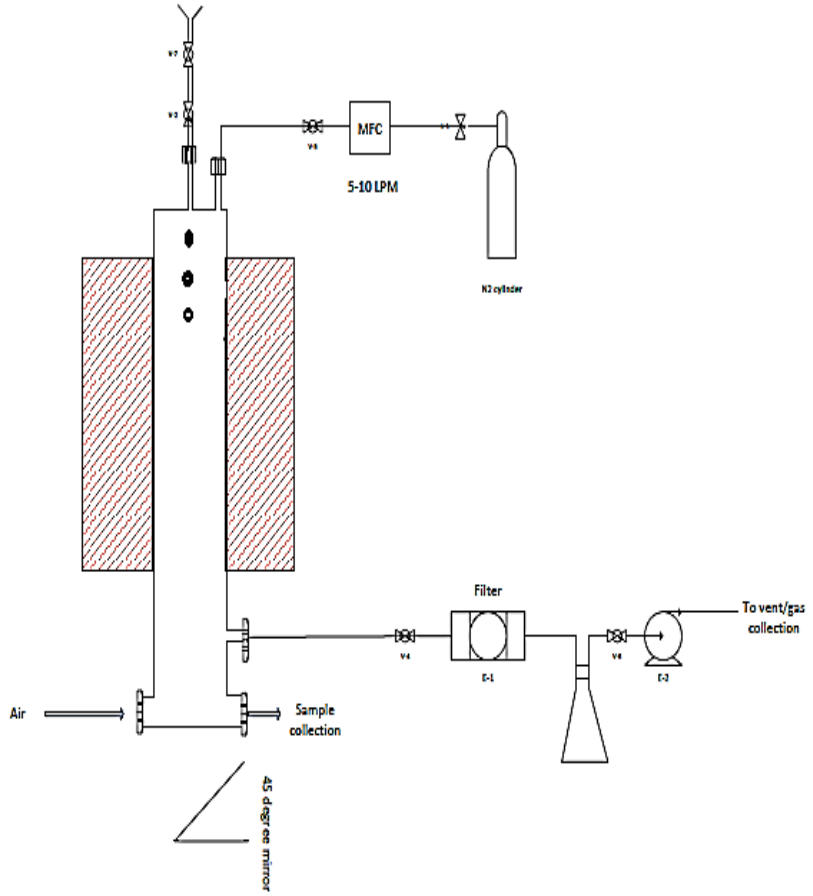

Figure 3.3: Schematic representation of entrained bed furnace used for pyrolysis and partial oxidation

3.2. Char Preparation

Asphaltenes sample were obtained from deasphalting unit of Nexen Energy ULC near Fort McMurray in Alberta. Asphaltenes samples obtained were solid and black in color with shiny surface character. Solid feeding of asphaltenes is preferred in the atmospheric drop tube furnace. For this, the solid samples were manually grinded using mortar and pestle and sieved to obtain specific cut fractions. Six cut sizes covering large particles 1.4-1.7*mm*, 1.0 -1.4*mm*, 0.85-1*mm*, intermediate size 425μm-0.85*mm*, 355-425μm and smaller particles 250-355μm were obtained. The furnace was operated at 600°C, 700°C, 800°C and 900°C for pyrolysis experiments. The furnace was heated at the rate of 15°*C/min* till the

required temperature and maintained at it for the experiments. Flow rate of N_2(99.998% purity) was maintained at 5*LPM* and 10*LPM*, however for later experiments it was kept at 5*LPM* for better entrainment of feed particles. After each experiment pyrolyzed char samples were collected from the bottom of the quartz tube. THF or toluene was used to clean the tube after each experiment to prevent contamination of samples by previous tars adhering to lower cooler zones in the tube.

3.3. Characterization of Char

Thermogravimetric analysis of char was conducted to determine the amount of volatile matter remained after pyrolysis. TA instruments SDT Q600 was used for such determination. About 5*mg* of char sample was placed in alumina crucible and heated to 800°C at heating rate of 15°*C/min*.in presence of N_2 .The percentage of weight loss suggested the volatile matter that remained unreacted during pyrolysis.

Surface morphology of char was studied using Zeiss Evo MA 15 LaB_6 filament scanning electron microscope. Secondary electron images were obtained using Everhart-Thornley detector. Few micrograms of char samples were placed on the carbon tape which was glued to SEM stub. The stub was then air blown to remove any loosely clinging particles. Subsequently the samples were carbon coated in Leica EMSCDE005 to improve imaging. Carbon coating inhibits charging and improves the capability of secondary electron signal to give a detailed topography. For cross sectional analysis few particles of char were dispersed in a mixture of West System 105 epoxy resin and West System 205 hardener. Exact proportion as mentioned in manual was taken in plastic container and mixed with care to avoid formation of air bubbles. Then it was poured in molding caps with char samples placed at bottom. The mixture was allowed to set overnight for proper curing. All specimens were ground at 100*RPM* in running water with SiC grit paper subsequently with 320, 400, 600,800, 1200 grits. This was followed by polishing using 1 micron water soluble polycrystalline diamond suspension.

FTIR is a high speed, sensitive tool used to get insight of functional groups in chars. It works on principle of absorption of infrared radiation from molecular stretching and bending vibration of the characteristic functional groups. FTIR spectra were recorded in MB3000-PH spectrometer in transmittance mode. Each result was obtained after accumulation of 120 spectral scans with resolution of 4 cm^{-1} in the spectrum range of 4000-400cm^{-1}. Range below 600cm^{-1} was omitted due to high disturbance. For analysis about 1*mg* of finely ground asphaltenes and char samples was placed under the probe. Semi-quantitative method was employed to compare the presence and absence of certain bonds present with varying temperature and particle size.

High carbon content in char samples makes it difficult for detection of inorganic matter through techniques like EDX, XRF or ICPMS. Drying ashing was preferred method for elimination of organic content in char. Char obtained from pyrolysis were heated in muffle furnace at 450°C for 6*hrs* till no further change in mass was observed. Ash obtained from muffle furnace was used for EDX and ICPMS analysis. Such low temperature was chosen for ashing so that the Na and K content does not change due to evaporation of sodium and potassium bearing species

EDX analysis was carried in similar fashion as SEM in the same instrument where results were acquired with a Peltier cooled 10mm^2 Bruker Quantax 200 Silicon drift detector with 123 *eV* resolutions. For ICPMS about 0.02*g* of ash was taken in a covered beaker to which 8*ml* HF, 2*ml* HNO_3 was added and then left on hotplate at 130°C for 48*hrs*. The cap was then removed and left at 140°C until completely dry. To this 5*ml* of HCl and 5*ml* of HNO_3 was added and heated at 130°C for 24*hrs* in covered condition. Again similar drying condition was applied. After completion of drying, 10*ml* of 8N HNO_3 was added with continued heating at 130°C. About 1*ml* of this mixture was pipetted out and to which 0.1*ml* HNO_3,

8.8 *ml* deionized water and 0.1*ml* internal standards (In, Bi and Sc) were included. This final mixture was used for analysis.

3.4. Partial Oxidation Experiments

Combustion experiments were carried out at furnace temperature of 700°C, 800°C and 900°C and particle residence time in range of 3-4*s*. Particle size of 425μm-0.85*mm* was considered for this study. Four binary mixtures of O_2 and N_2 were compared: 1% O_2 - 99% N_2, 2% O_2 - 98% N_2, 5% O_2 - 98% N_2 and 21% O_2 - 79% N_2. For initial experiments O_2 was derived from oxygen (99.5% purity) containing cylinder. However it led to complete combustion at high temperatures. Later, extra dry air was substituted in place of oxygen with appropriate stoichiometric calculations for controlled combustion reactions. Burnout was determined using ash tracer method an analytical method used to determine carbon conversion during combustion.

3.5. Char Combustion Kinetics

The experiments were performed using TA instruments SDT Q600 thermogravimetric analyzer. To maintain combustion condition high purity air at 50*ml/min* was used as carrier gas. About 5-6*mg* of char samples obtained from pyrolysis of asphaltenes size fractions 425μm-0.85*mm*, 355-425μm and 250-355 μm at 700°C and 800°C was placed in the alumina crucible. For all cases five different heating rates 2.5, 5, 7.5, 10 and 12°*C/min* was considered. The weight loss curve was used for activation energy calculation using Isoconversional technique.

Chapter 4
RESULTS AND DISCUSSIONS

4.1. Char Yield and Composition from Pyrolysis Experiments

4.1.1. Char Yield

The yield of char from pyrolysis experiments was calculated from the following equation as based on mass balance:

$$char\ yield(\%) = 100 \times \frac{weight\ of\ char\ collected}{weight\ of\ feed} \tag{4.1}$$

Char yield at 600˚C was high for particles size 0.85-1.7mm. With increase in furnace temperature the yield decreases. This indicated that larger particle size needed longer residence for complete reaction. Hence for particle size below 0.85mm, all experiments were carried upto temperature of 900˚C and those at 600˚C were neglected. For lowest particle size the char yield reduced significantly to 1.08% at 900˚C. At 900˚C the yields for 355-425μm and 250-355μm sizes were almost similar. The decrease in char yield with increasing temperature could be related to primary decomposition or secondary decomposition of char residue [94].

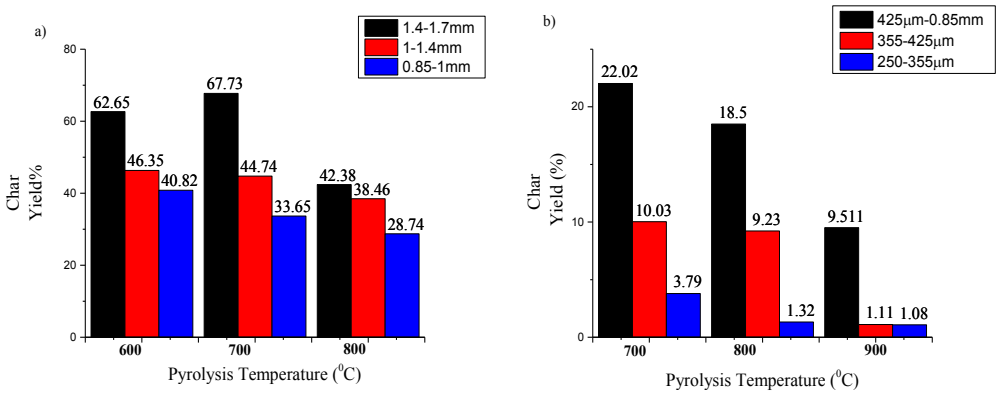

Figure 4.1: Char yield at varying furnace temperature: a) High sizes b) Low sizes particle

4.1.2. Thermal Analysis of Char

The high char yield at lower temperature and higher particle size could be explained by high volatile matter remaining in char. This was demonstrated from

the thermogravimetric analysis of the char obtained. Low char yield for range 250-355μm at 900°C had low volatile content (Figure 4.2 b) illustrating appropriate devolatilization while 1.4-1.7mm size particle at 600°C had most of the volatile matter still intact suggesting poor devolatilization(Figure 4.2 a).

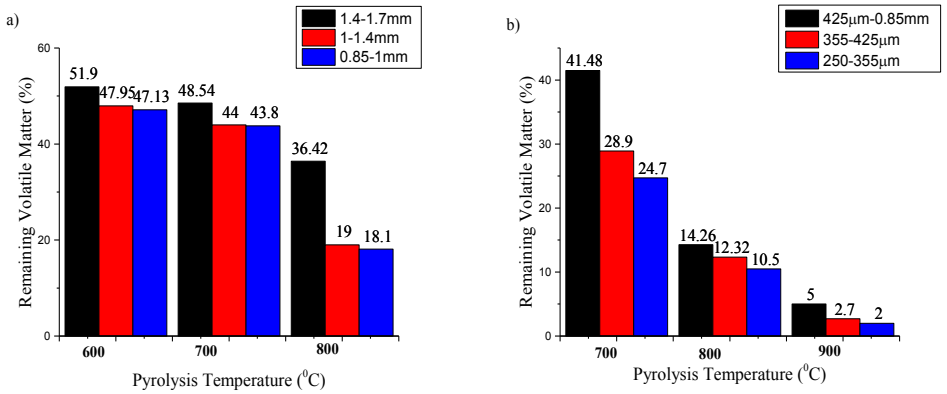

Figure 4.2: Volatile matter remained in char collected: a) High sizes and b) Low sizes

4.1.3. Functional Groups in Char

Effect of temperature on the structure of char was studied by varying particle size from 1-1.4mm, 425μm-0.85mm and 250-355μm. Figure 4.3-4.5 represented the FTIR spectra of asphaltenes and char obtained for various size at different pyrolysis temperature. All the variations in structure could be categorized as follows:

Changes in Aliphatic structures: The stable C-H stretching in 3000-2840cm^{-1}, C-H ending vibration at 1473cm^{-1} and 1375cm^{-1} along with methylene rocking at 720cm^{-1} indicated the presence of straight chain alkane of seven or more carbon atoms in asphaltenes as well as its char at all the temperatures. Chars obtained from 1-1.4mm asphaltenes at 700˚C had similar absorption arising for C-H stretching and bending in alkanes. However the intensity of the alkane band decreased with pyrolysis temperature. Moderate to weak C=C stretching of unconjugated alkenes along with strong absorption of $=CH_2$ wagging could be observed at 1667-1640cm^{-1} and 840cm^{-1} respectively. Alkene presence decreased for char obtained from 425μm-0.85mm asphaltenes at 700˚C, 800˚C,900˚C and

for char obtained from 250-355μm asphaltenes at 700˚C. But the intensity slightly increased for char obtained from 250-355μm asphaltenes at 800˚C and 900˚C.

Changes in Aromatic structures: The most characteristic absorption bands resulting from C-H out of plane bending occurred in 870-675cm^{-1} zone. For chars from 1-1.4mm asphaltenes size, there was not much change with temperature. However this zone drastically decreased for chars from 425μm-0.85mm at pyrolysis temperature 700-900˚C and that of chars from 250-355μm at 700˚C. This trend indicated that larger aromatic rings formed due to aromatic substitution decreased with pyrolysis. For chars from 250-355μm asphaltenes, the region around 873-735cm^{-1} increased at pyrolysis temperature of 800˚C and 900˚C . It was because of the rapid release of volatiles the free H radical got stabilised. Moreover at high temperatures there might be an increase in degree of aromatic condensation and formation of larger aromatic nuclei [95].

Changes in Oxygen containing structures: C=O stretching absorption band from 1870-1540cm^{-1} was an implication for ketones, aldehydes and carboxylic acids. Moderate absorption in 1300-1100cm^{-1} as a result of C-C-C stretching and C-C(=O)-C bending illustrated the presence of ketones. Oxygen was also distributed in form of aldehyde which was evident from aldehydic C-H stretching at 2830-2695cm^{-1} with first overtone of C-H bending near 1370cm^{-1}. Characteristic C-O-C stretching vibration at 1085cm^{-1} was seen for chars obtained from 1-1.4mm, 425μm-0.85mm asphaltenes at 800˚C. At temperature above 800˚C ether bond was unstable [95].

Absence of band at higher wavenumber like 3000cm^{-1} implied the absence of O-H and N-H functional groups. Hence the possibility of oxygen occurring in the form of carboxylic acid or alcohol was ruled out.

With increase in temperature the C=O and C-O bond was destroyed. From the absorption spectrum it was known that C=C and C=O overlap with one another.

The loss of C=O and C-O bonds made C=C symmetrical and hence IR spectra became inactive. Decarboxylation and Decarbonylation reactions at higher temperatures lead to crosslinking forming more stable C=C structures and alkyl-aryl C-C forms. However rapid release of volatiles at high temepratures resulted in loss of active sites symbolizing lower combustion and gasification rates [95][96].

Changes in Sulfur containing structures: S-H stretching vibrations at 2600-2550cm^{-1} was absent and mostly obscured by strong carbonyl absorption. But sulfur was present in asphaltenes and char in form of C=S (thiocarbonyl) which was evident from 1250-1020cm^{-1} zone. This region also had C-O and C-N stretching , hence considerable interaction between these vibrations in a single molecule was expected. Presence of sulfur decreased with pyrolysis temperature but was more perceptible in case of char obtained from 250-355μm asphaltenes.

Changes in Nitrogen containing structures: The absorption spectra at 1576-1429cm^{-1} were mostly weak and demonstrated the presence of polar N=N bond. There was no significance change in this region with pyrolysis temperature. Nitrogen was also distributed in form of nitriles as demonstrated by 2300-2210cm^{-1} absorption stretch. Presence of nitrile groups in asphaltenes or chars from 1-1.4mm asphaltenes could not be noticed. However when temperature was above 700°C for chars from 425μm-0.85mm and 250-355μm asphaltenes the amount of nitrile group present increased. The appearance of nitrile groups at high temperature was an indication of rupture of complex porphyrnic structures. Absence of O-H functional group in char also prevented the conversion of nitrogen in the rings into N-H forming structure [97]. Hence the possibility of C≡N structure increased. Presence of organically bound nitrogen had adverse effect on the performance of catalyst in fluid catalytic cracker units due to ability of attacking the active sites in any catalyst used for cracking.

It would be meaningful to notice that most of the polar groups presence was negligible for asphaltenes as the high polarity is attributed to existence of

porphyrins and their complexes with transition metal ions such as vanadium and nickel [98].

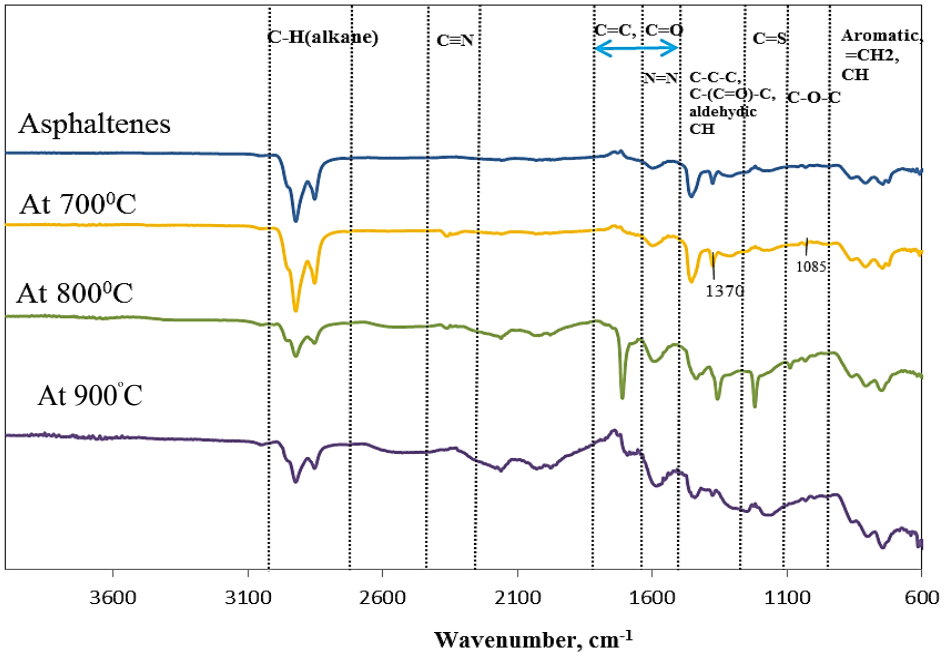

Figure 4.3: FTIR spectra of asphaltenes and char from 1-1.4mm particle size

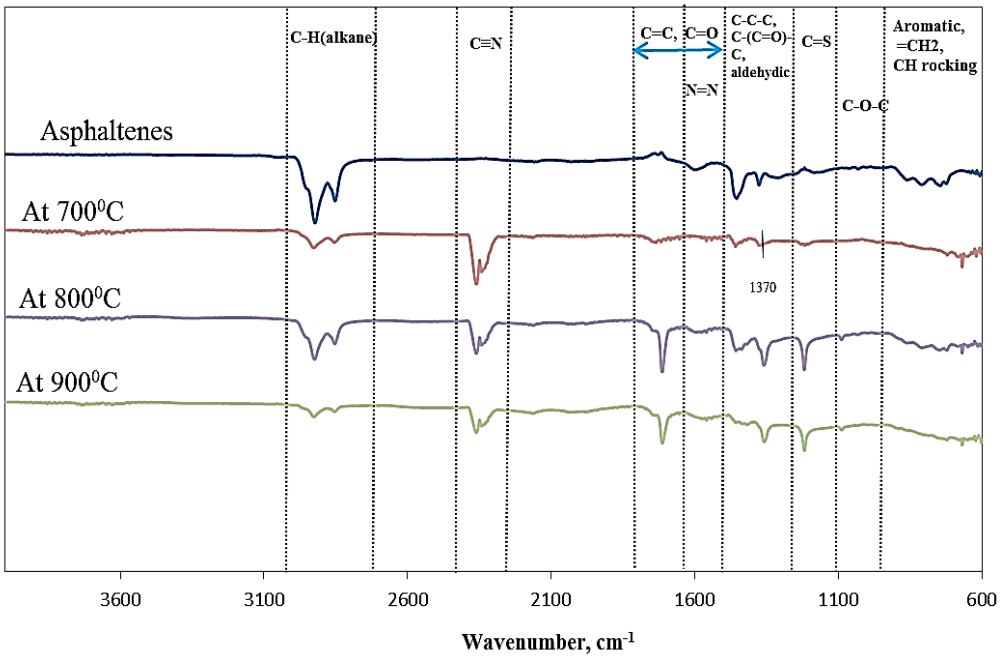

Figure 4.4: FTIR spectra of asphaltenes and char from 425µm-0.85 mm particle size

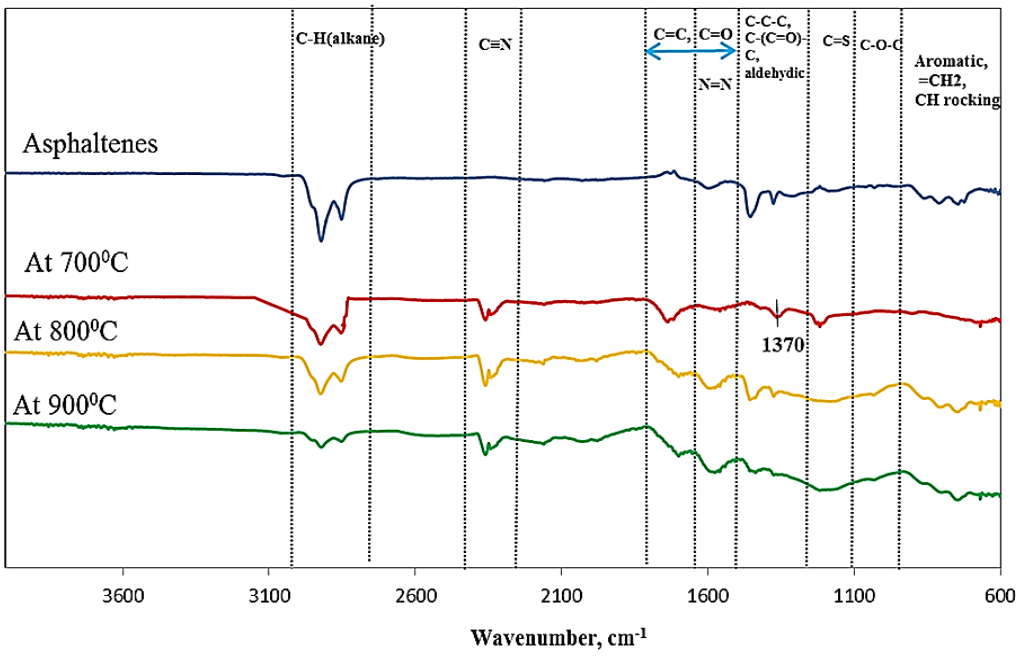

Figure 4.5: FTIR spectra of asphaltenes and char from 250-355µm particle size

4.1.4. Mineral Matter in Char

Ash content for char at pyrolysis temperatures 700°C and 900°C of sizes 425μm-0.85mm and 355-425μm was plotted as shown in Figure 4.6. As contrast to char yield, the ash content increased significantly with pyrolysis temperature and with decrease in particle size [99]. It was also noted that the feedstock had lower ash content than corresponding char. During pyrolysis the volatile release led to structural transformation such as collapse of weakly bound organic structures as confirmed by FTIR study. The complex organically bound metal ions transformed to free ions and with ashing conditions formed heavy metal oxides leading to increased ash content with pyrolysis temperatures. It was noted that 80-90% of the metals in crude were concentrated in its asphaltenes with 25-35% in porphyrin structures and remaining as organically bound [100]. Weak nature of organically bound metals such as V, Ni caused easy release at given pyrolysis temperature .Presence of mineral matter in ash/char was essential for their catalytic effect and influence in increased reactivity [101].

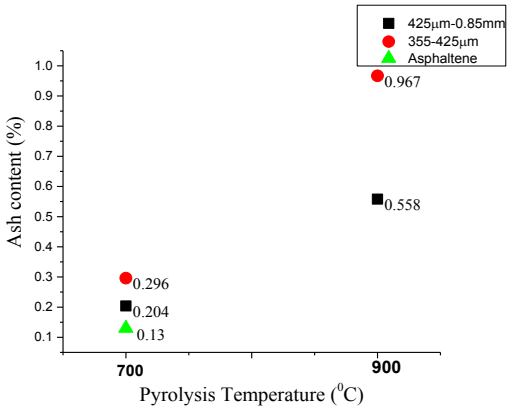

Figure 4.6: Ash content in asphaltenes and char

Bulk EDX of the ash samples gave a semi-quantitative knowledge of the mineral matter concentrated. Figure 4.7 represented the area of ash sample under consideration. EDX analysis exhibited uniform distribution of transition metals such as V and Ni at all conditions. Presence of small quantities of alkali metals like K, Ca and Na might lead to corrosion in pipelines and furnace wall.

Examination the ash structure from Figure 4.7 revealed fused like state which was mostly due to combination of Al and Si. Existence of Al and Si might either be due to trace quantity of clay or sand in original asphaltenes sample or due to contamination by insulating Fiberfrax material. Table 4.1 represented the elemental composition obtained from EDX analysis.

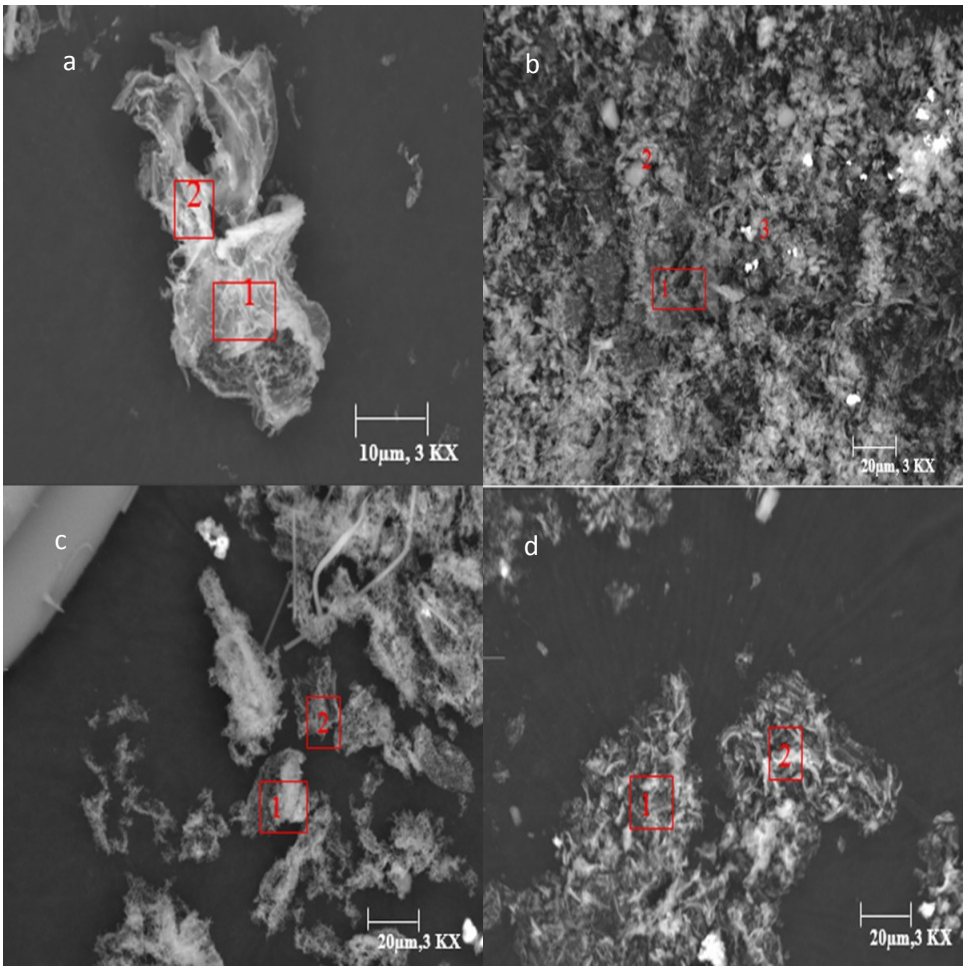

Figure 4.7: SEM of ash obtained; a-b: 425µm-0.85mm size at 700˚C and 900˚C pyrolysis temperature, c-d: 355-425µm size at 700˚C and 900˚C pyrolysis temperature respectively

Table 4.1: EDX elemental data for chars obtained

Elements(*wt.*%)	425μm-0.85mm				355-425μm			
	700˚C		900˚C		700˚C		900˚C	
	1	**2**	**1**	**2**	**1**	**2**	**1**	**2**
C	45.55	42.77	55.74	55.94	54.77	57.36	62.81	68.59
O	35.29	34.95	30.55	27.16	31.53	29.99	27.17	23.90
Al	1.09	1.56	-	-	0.89	0.49	-	-
Si	1.04	1.56	0.35	0.49	0.82	0.59	-	-
S	0.37	0.44	-	-	0.24	0.27	-	-
K	0.16	-	-	-	-	-	-	-
Ca	1.026	0.27	-	-	0.24	-	-	-
V	11.43	13.10	9.95	11.72	8.17	7.96	6.69	5.26
Fe	0.33	0	-	-	-	-	-	-
Ni	4.43	5.34	3.40	4.69	3.34	3.34	3.33	2.25

Accuracy of EDX analysis was questionable as it gave elemental analysis for a given area under study. Larger part of the sample and elements remained undetected. Hence ICP MS analysis was carried as it was not only sensitive to elements lighter than Al such as Be, Li, B but also detected light elements in presence of heavier ones as illustrated in Figure 4.8 and 4.9.

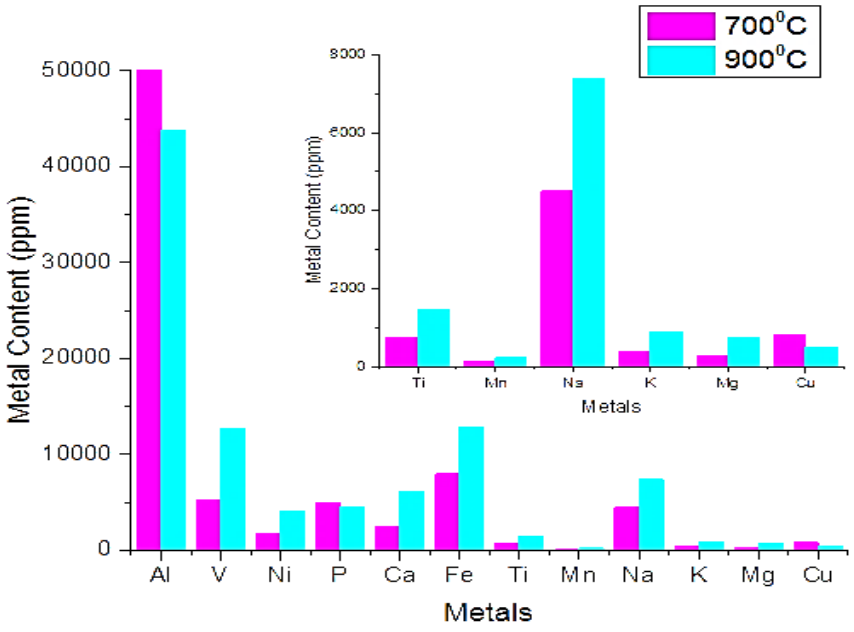

Figure 4.8: Metal content in 425µm-0.85mm size char ash from ICPMS

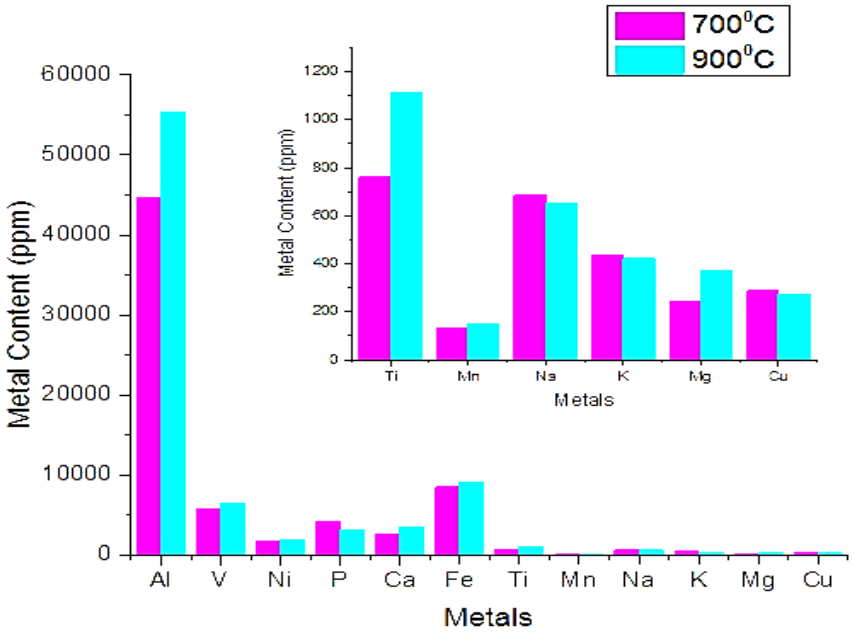

Figure 4.9: Metal content in 355-425µm size char ash from ICPMS

Metals like Mn, Ti, Mg and Cu were also detected using ICP MS. For both particle sizes, the inorganic content increased with pyrolysis temperature. Uniform distribution of V and Ni might lead to accumulation and deposition on catalyst which had impact on high char production as well as catalyzed combustion process to forming CO_2 rather than CO[100]. Presence of K and Na was also evident at high pyrolysis temperature (900˚C) even when the volatilization of alkali salts might occur at low temperatures. Alkali metals present in asphaltenes could be classified as organically bound, inorganically bound ,complex inorganically bound(like $Na_2Si_2O_5$) and stable forms(present in organic matrix covered by carbon or alumina-silicates) [102]. Below 700°C release of K was mostly due to decomposition of organically associated K. Above 800°C emission of K could most probably be based on vaporization of K-phosphates as well as stables forms of K-silicates(melting points between 810-850°C). Na might have followed the similar release mechanism as K. However there might be an increase in Na species for size 425μm-0.85mm at 900°C due to formation of stable $NaAlSiO_4$ and $Na_2Si_2O_5$ [103][102] . Plot between ratios of alkali metals to transition metals (Figure 4.10-4.11) indicated evolution of Na and K at higher pyrolysis temperatures. Removal of Na seemed faster than the K under similar conditions.

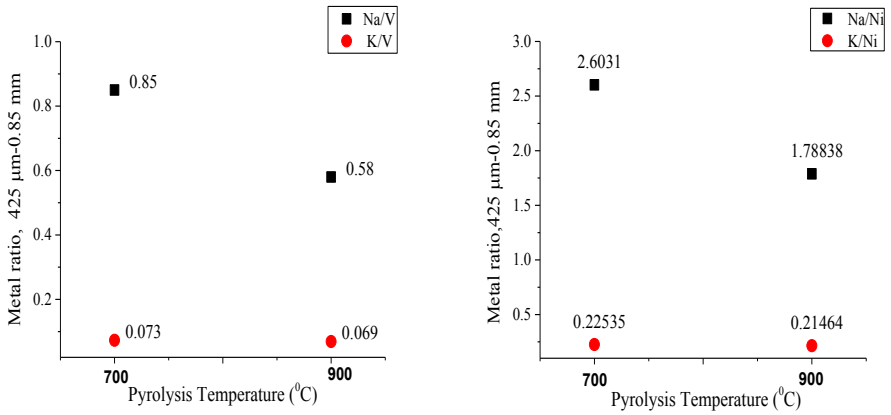

Figure 4.10: Alkali and transition metal ratio vs pyrolysis temperature for 425µm-0.85mm

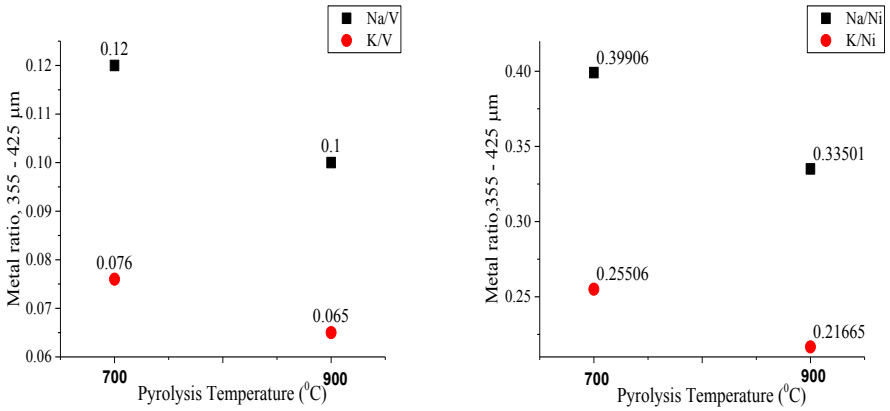

Figure 4.11: Alkali and transition metal ratio vs pyrolysis temperature for 355-425µm

4.2. Morphological changes in Char from Pyrolysis Experiments

Morphology of char collected for size range of 0.85-1.7*mm* at all pyrolysis temperature demonstrated the similar structure as that of parent asphaltenes (Figure 4.12). However at 900°C for 425μm-0.85*mm* size, the chars turned irregular and flaky. As the size reduced below 425μm notable changes were recorded at different pyrolysis temperature.

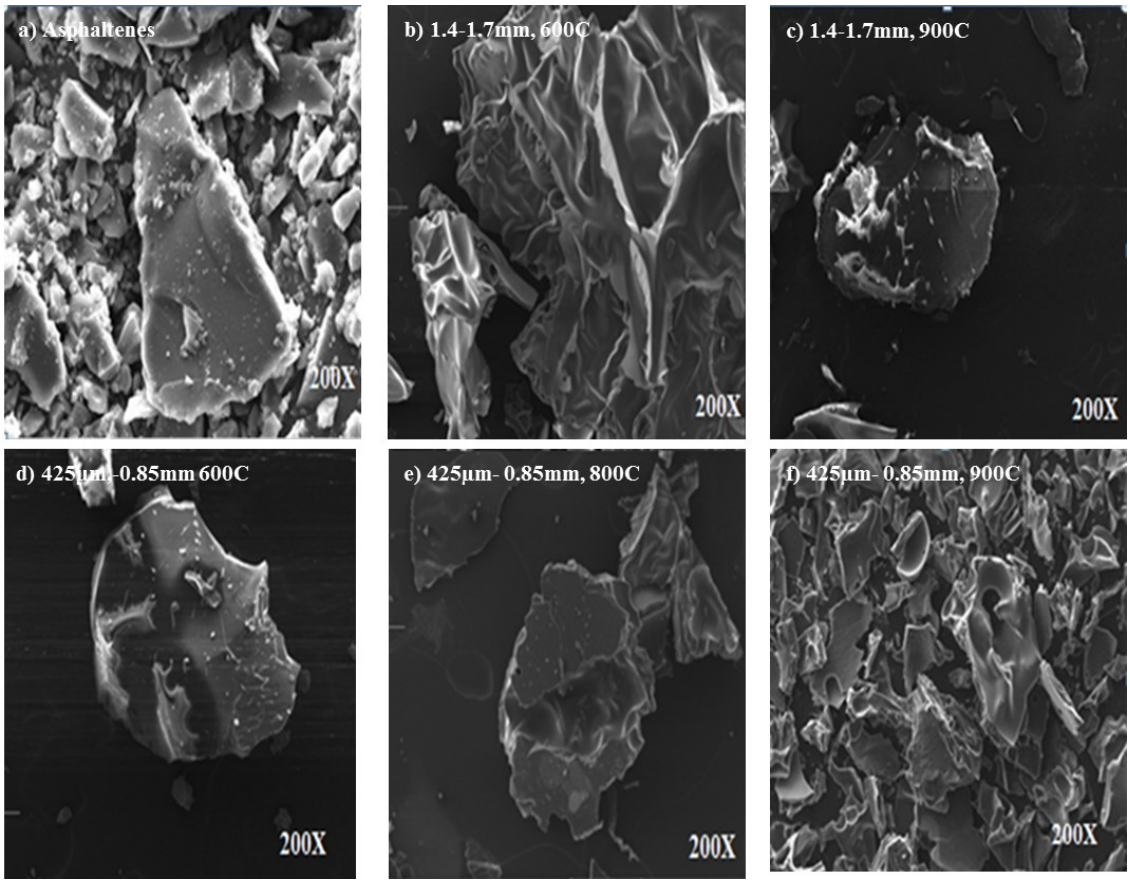

Figure 4.12: SEM of: a) Raw asphaltenes, b)-c) char from 1.4-1.7mm at 600˚C and 900˚C, d)-f) char from 425µm-0.85mm at 600˚C, 800˚C and 900˚C

At 700°C for size 355-425μm, the chars formed solid spheres with thick boundaries. At 800°C, the chars obtained were light and porous with a central void. Cross-sectional SEM depicted large bubbles with thin walls (Figure 4.13). At 900°C, chars formed cenospheres with defined ribs. Such types of chars were classified as "Group C" chars or chars with honeycomb structure. At this condition there was prominent increase in bubble formation (Figure 4.14).

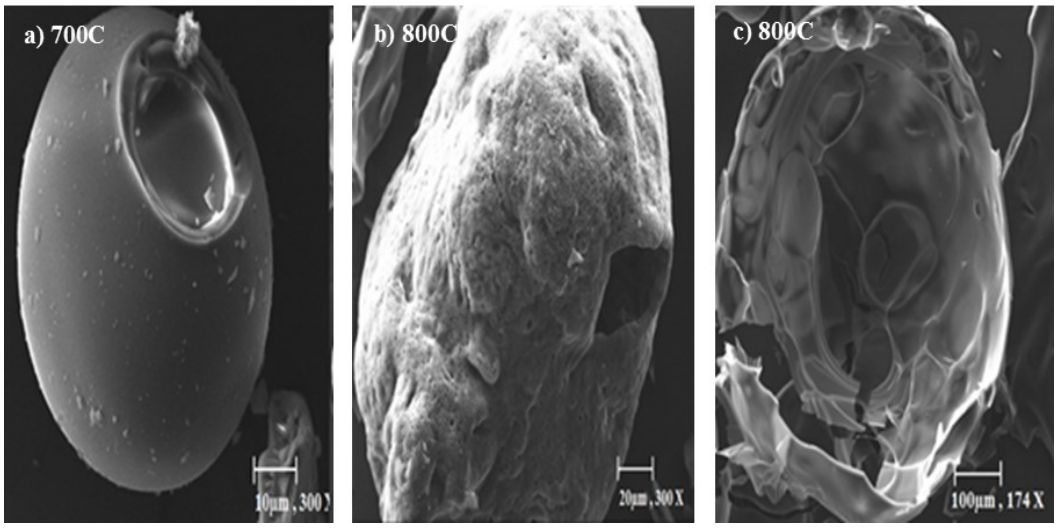

Figure 4.13: a) SEM of char from 355-425µm size obtained at 700˚C , b) 800˚C, c) cross-sectional view at 800˚C

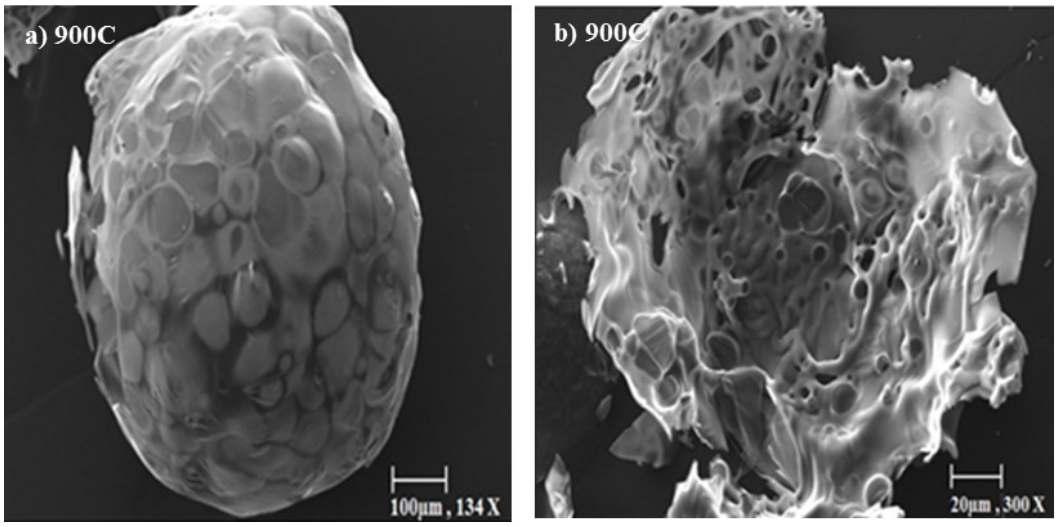

Figure 4.14: a) SEM of char from 355-425µm size obtained at 900˚C b) cross-sectional view

At 700°C for 250-355μm size feed, the cross-sectional analysis indicated bubble formation along thick wall. At 800°C, for same size the chars developed a round smooth structure with single central void. Such structures belonged to "Group A" chars called Cenospheres[66].The cross-sectional SEM exhibited numerous

mesopores with irregular pore boundaries. Small pores seemed to be embedded in the walls separating the larger cavities. The thickness of wall could be estimated from *ImageJ* as below 5μm. Existence of bubble indicated that some volatile matters were still trapped in the given char.

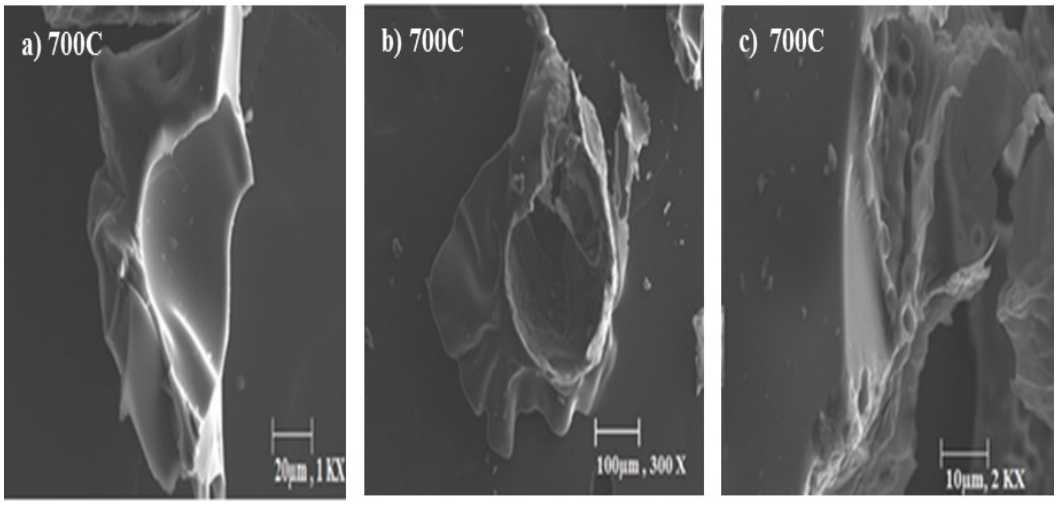

Figure 4.15: a) SEM of char from 250-355µm size obtained at 700°C, b) cross-section, c) details on wall

At 900°C, the cenospheres developed a rugged exterior with increased mesopores. This was probably due to rapid release of volatiles. Some of these mesopores coalesced to form larger macropores. No bubbles were observed suggesting that maximum volatile species had been liberated. Few particles illustrated cracks and fragmentation which was crucial to high amount of ash formation.

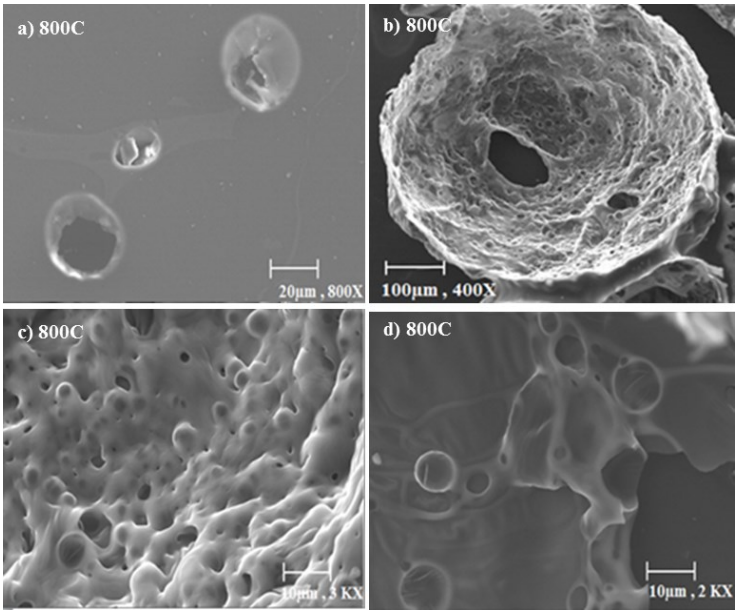

Figure 4.16: a) SEM of char from 250-355µm size obtained at 800˚C,b) cross-section, c) bubble formation, d) details on wall

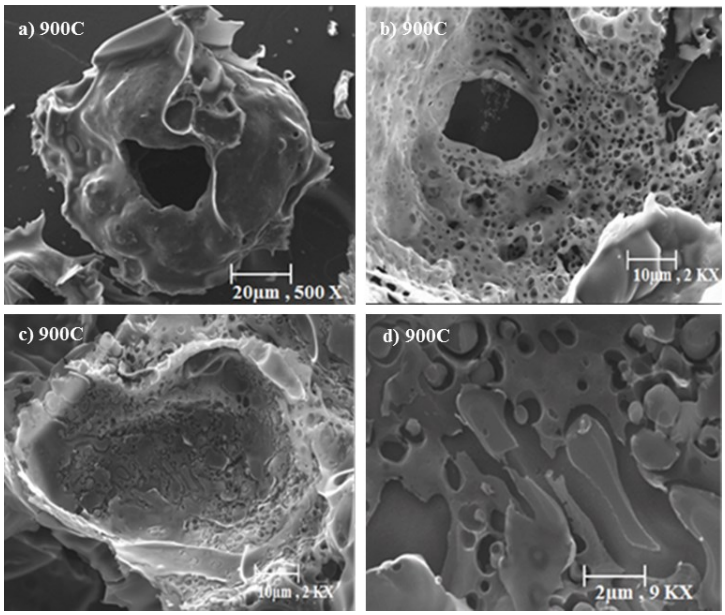

Figure 4.17: a) SEM of char from 250-355µm size obtained at 900˚C,b) cross-section, c) fragmentation d) fragmentation details

4.3. Combustion Experiments

4.3.1. Char Burnout

Partial oxidation experiments were important in understanding the removal of condensed tar on chars formed. The crucial variable characterizing partially oxidized sample was burnout or carbon conversion. The burnout percentage was calculated using equation 2.7. The burnout of $425\mu m$-$0.8mm$ asphaltenes size increased with oxygen partial pressure. But it was interesting to notice that burnout of 2% O_2 was lower than 1% O_2 partial pressures. At furnace temperature of 900°C the burnout for partial pressures of 1%, 2% and 5% were almost similar indicating most of the volatile had been detached by the time the particles reached 900°C. However it was difficult to collect the char samples at 900°C for 21% O_2 partial pressure due to ignition of collected samples.

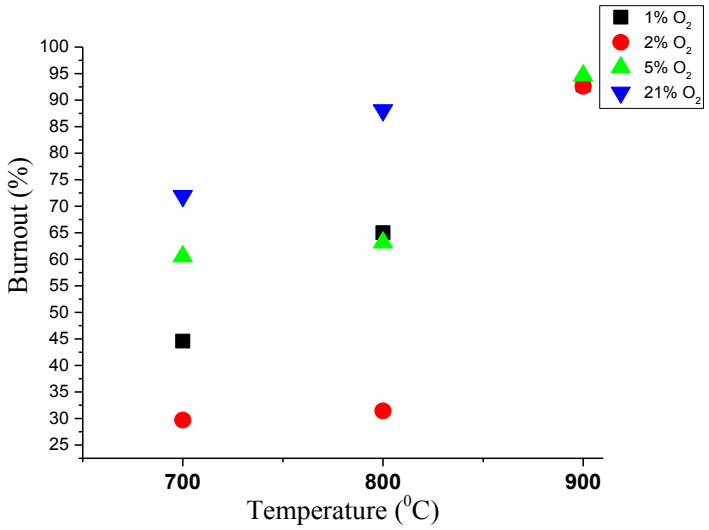

Figure 4.18: Burnout profile of 425µm-0.85mm asphaltenes at different oxygen partial pressure

Due to low volatilization of trace elements during ashing the burnout profiles obtained might be erroneous. Hence, simple mass balance method could also be used to indicate the char yield when pure N_2 was replaced by partial O_2 pressures (Figure 4.19).

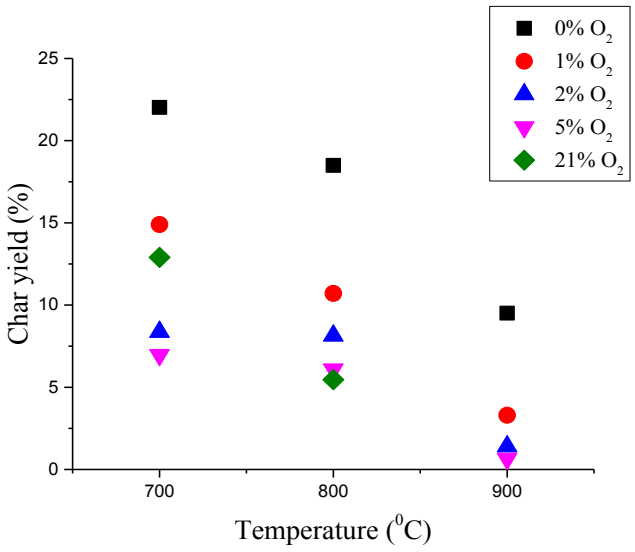

Figure 4.19: Yield of char from 425µm-0.85mm asphaltenes at different oxygen partial pressures

4.3.2. Morphology of Char obtained from Combustion

Morphology of char obtained for 1% O_2 partial pressure at 700°C demonstrated similar features as those obtained for pyrolysis conditions at 900°C. At 900°C the char obtained had evidence of oxidation on the surface with small bubbles developing (Figure 4.20). For 2% O_2 partial pressure and at 900°C the char turned flaky with tortuous structure developing around as noticeable in Figure 4.21. The tortuous structure was more evident from Figure 4.22 for 5% O_2 partial pressure at both 700°C and 900°C. At partial pressure of O_2 above 2%, char particles tended to fragment into smaller fractions. In presence of air, the morphology changed from thick swollen structure to thin fragments with numerous pore type formations. There was no evidence of tar accumulation on the surface of char for high furnace temperature and O_2 partial pressure.

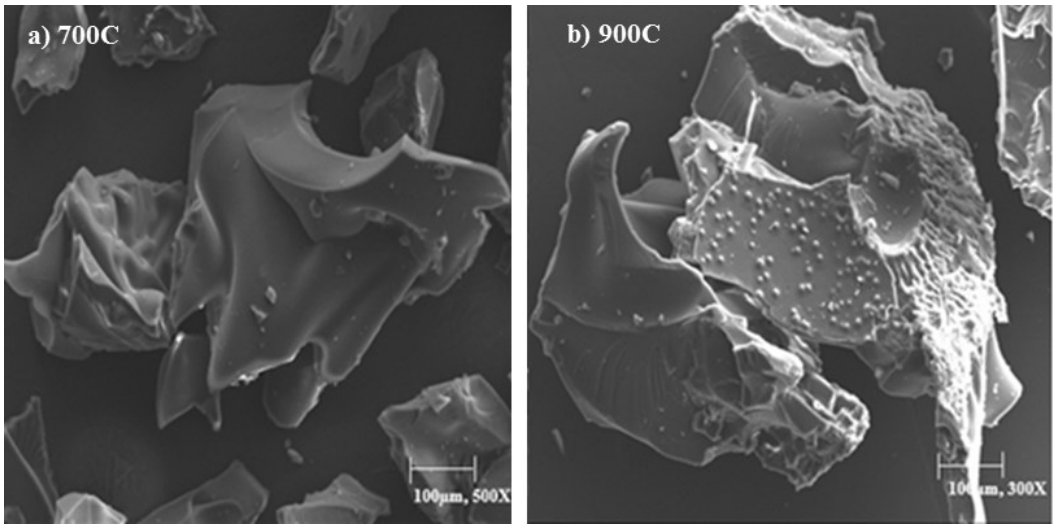

Figure 4.20: SEM of char formed in presence of 1%O_2 partial pressure: a) 700˚C, b) 900˚C

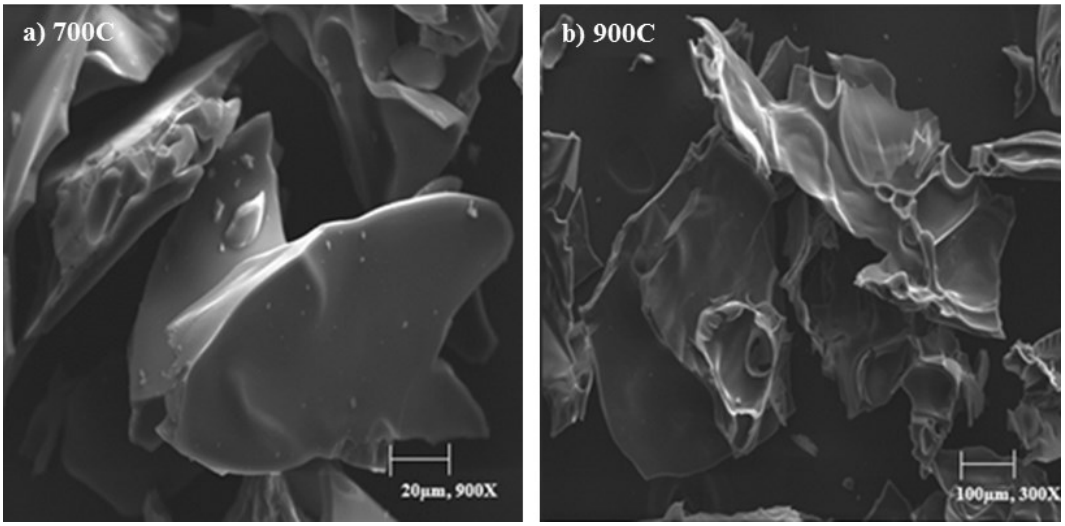

Figure 4.21: SEM of char formed in presence of 2%O_2 partial pressure: a) 700˚C, b) 900˚C

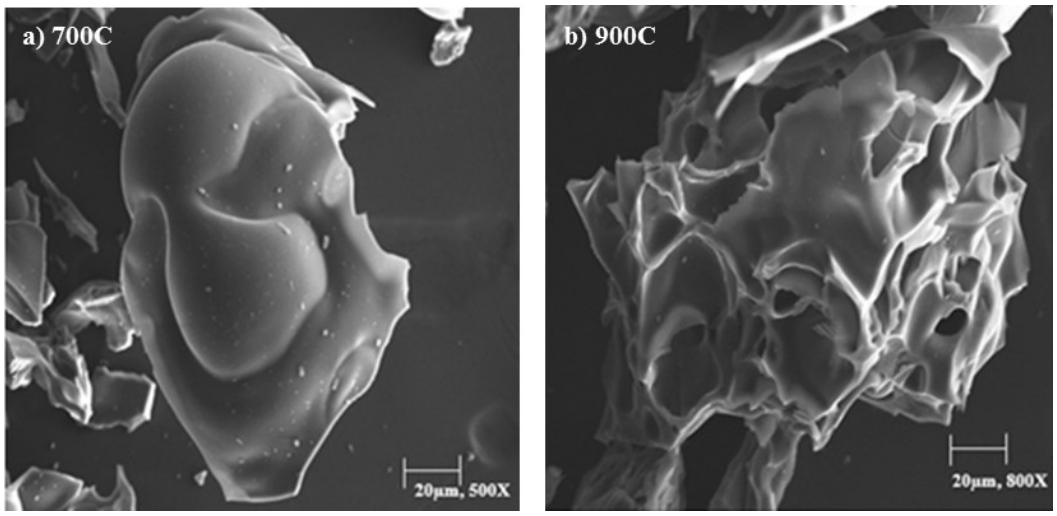

Figure 4.22: SEM of char formed in presence of 5%O_2 partial pressure: a) 700˚C, b) 900˚C

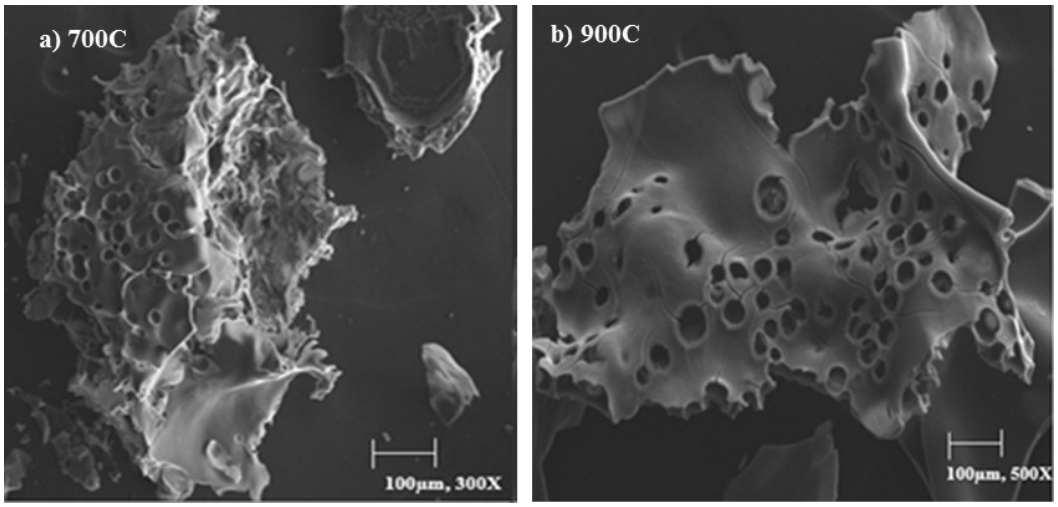

Figure 4.23: SEM of char formed in presence of 21%O_2 partial pressure: a) 700˚C, b) 900˚C

4.3.3. Effect of Char Morphology on Combustion rate

Calculation of combustion reactivities was considered complex because oxygen brought about additional reactions such as gas phase reactions between volatiles and oxygen , and heterogeneous combustion of remaining char formed [104]. The weight loss curve (TG) for 425μm-0.85mm size char obtained at 700˚C from DTF indicated two stages at all heating rates(Figure 4.24 a). The initiation of devolatilization and combustion of volatiles (stage A) remained in char took place

from 330-390°C while combustion of fixed carbon (stage B) in char commenced from 440-470°C. The burnout temperature for this case lied in range 490-550°C. The peak temperature for maximum evolution was indicated with the help of DTG curve (Figure 4.26). Peak temperature for gas phase reactions varied from 430-450°C while that of char gas reactions occurred between 450-530°C. The TG curves as well as peak temperatures in DTG shifted towards higher temperature. During high heating rates larger instantaneous energy was provided to the system for short period/reaction time, hence high temperature was required for decomposition. While for slow heating rates, longer time provided better heat transfer preventing any temperature gradient inside the sample. The weight loss curve (TG) for 425μm-0.85mm size char obtained at 800°C from DTF illustrated single stage at all heating rates (Figure 4.24 b).

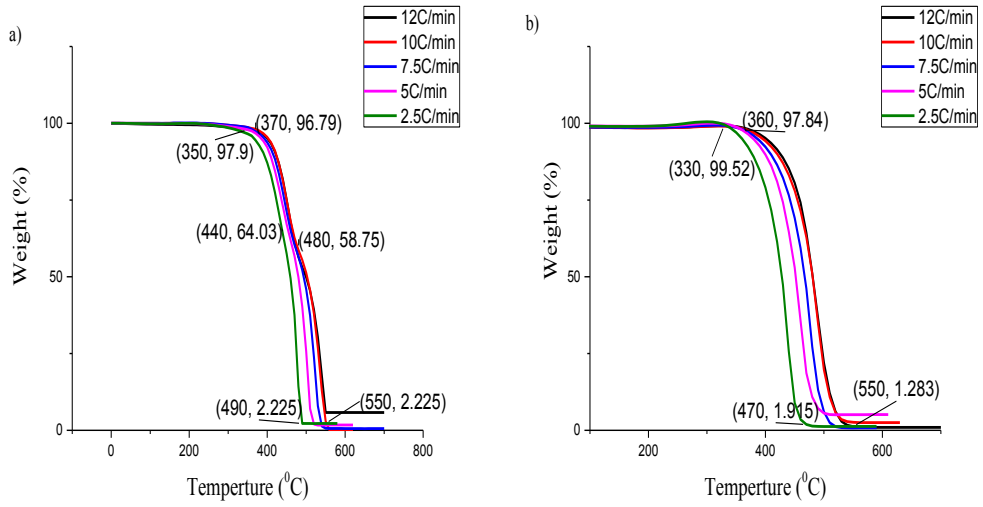

Figure 4.24: TG weight loss curve for 425µm-0.85mm size char obtained: a) 700°C, b) 800°C for five heating rates

The weight loss curve (TG) for 250-355μm size char obtained at 700°C from DTF indicated two stages at higher heating rates and single stage for 2.5-5°C/min (Figure 4.25 a). This could be associated with low volatile content remained after pyrolysis conditions. Moreover high heating rates encouraged simultaneous evolution and ignition of volatiles while low heating rates had evolution prior to

ignition. For chars collected at 800°C, the TG curve again revealed single stage of decomposition (Figure 4.25 b). Similar behavior was observed in case of 355-425μm size char obtained at 700°C and 800°C.

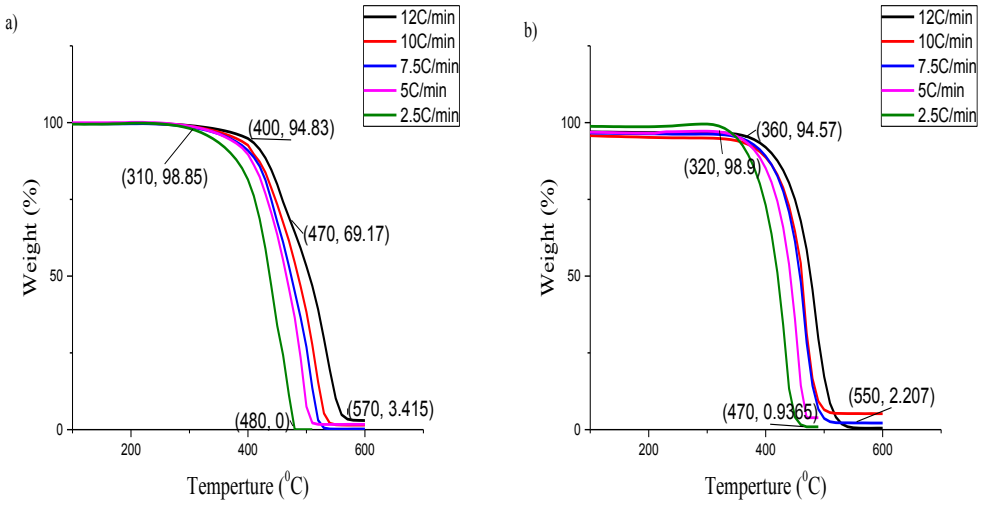

Figure 4.25: TG weight loss curve for 250-355µm size char obtained: a) 700°C, b) 800°C for five heating rates

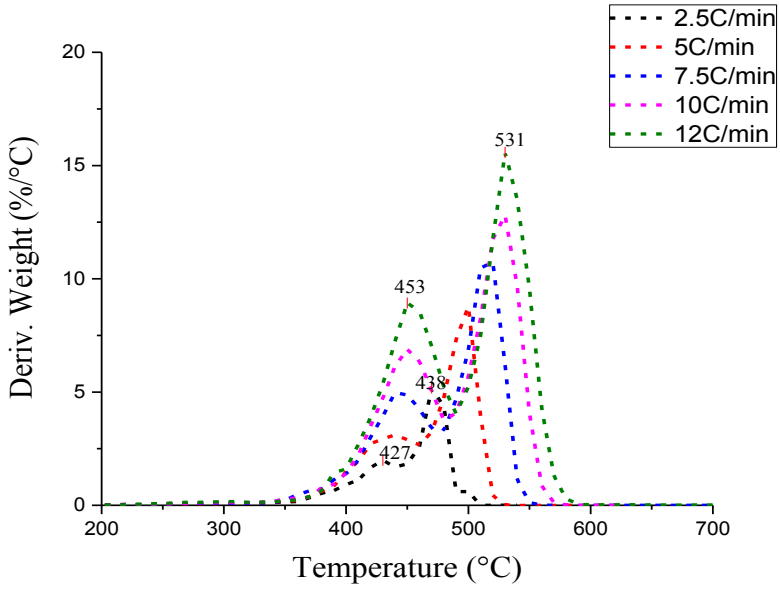

Figure 4.26: DTG curves for 425µm-0.85mm size char obtained at 700°C for five heating rates

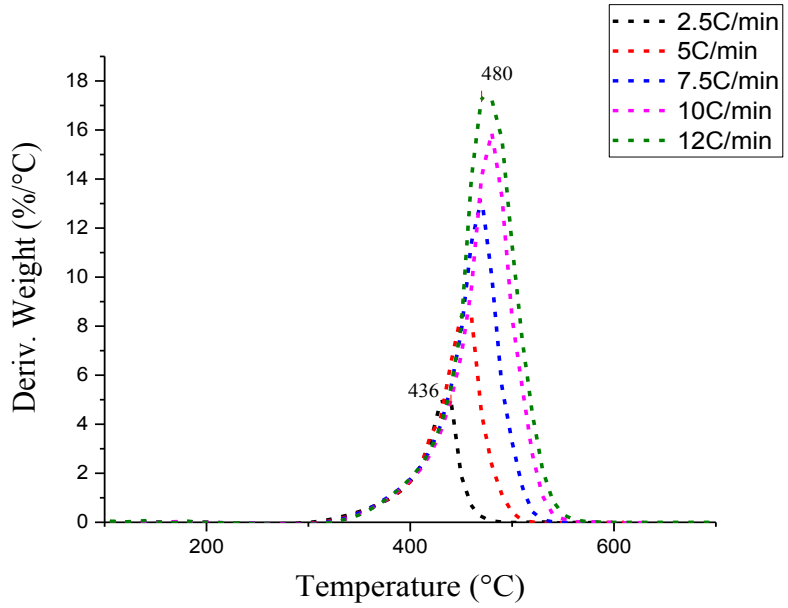

Figure 4.27: DTG curves for 425µm-0.85mm size char obtained at 800°C for five heating rates

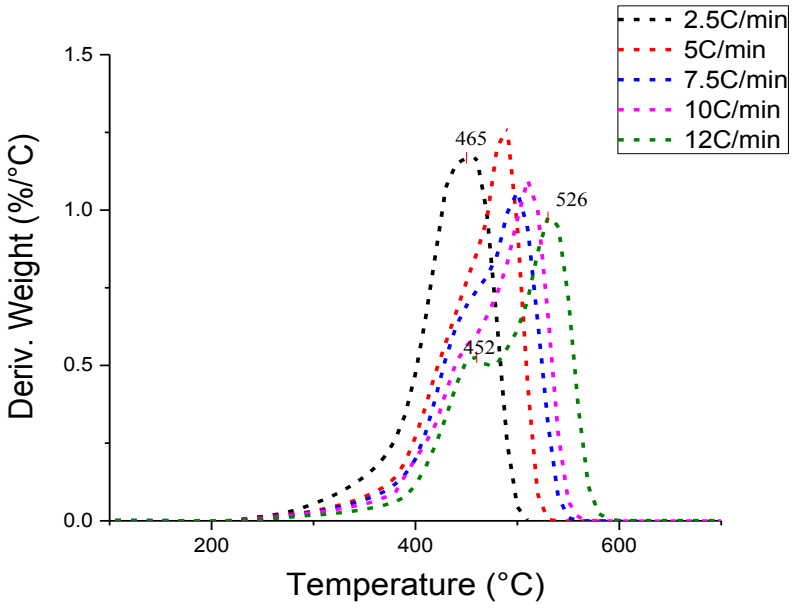

Figure 4.28: DTG curves for 250-355µm size char obtained at 700°C for five heating rates

The results obtained from TGA were elaborated to calculate kinetic parameters through model free method. Activation energy (E_a) served as an indicator for reactivity comparison between chars obtained at different pyrolysis conditions. FWO method was utilized to obtain apparent E_a at different conversion levels without assuming the actual reaction model. This was done by obtaining a plot between natural logarithm of heating rates (β) and 1000/T for individual conversions. The plots were linearly fitted to obtain the slope which was equated with $-1.052\times E_a/R$ stated in equation (2.14) to obtain the activation energy. The square of correlations coefficient for linear fitting varied from 0.9586-0.9997. Temperature range for the two stages and its peak value for all conditions were tabulated in Table 4.2.

Table 4.2: Temperature range and peak temperature for all samples

Particle size	Pyrolysis Temp (°C)	Heating rate (°C/min)	Temperature Range(°C)		Peak Temperature (°C)	
			Stage A	Stage B	Stage A	Stage B
425μm-0.85mm	700	2.5	362-438	438-492	427.3	474.2
		5	359-449	449-521	440.8	498.7
		7.5	352-464	464-540	447.5	516.2
		10	371-473	473-556	449.7	527.5
		12	365-477	477-574	453.7	531.2
425μm-0.85mm	800	2.5		326-475		435.9
		5		329-504		454.9
		7.5		340-523		472.5
		10		344-541		477.6
		12		352-547		480
355-425μm	700	2.5	308-441	441-483	435.8	466.5
		5	363-462	462-516	457.4	481.2
		7.5	370-474	474-539	462.2	496.6

		10	385-483	483-555	441.4	506.9
		12	396-477	477-584	450	527.4
		2.5		309-494		436.3
		5		311-512		460
355-425μm	800	7.5		333-543		462.2
		10		336-561		447.36
		12		348-565		481.2
		2.5	311-441	441-484	437.5	465.6
		5	348-468	348-468	454.7	489.1
250-355μm	700	7.5	377-478	478-530	467.7	494
		10	371-479	479-547	476.2	503.7
		12	387-474	474-574	452.5	526.2
		2.5		319-474		431.2
		5		333-496		448.5
250-355μm	800	7.5		346-518		458.3
		10		348-540		475
		12		358-547		475.7

It was observed that apparent activation energies calculated by FWO method was not similar for all conversion indicating complex multi-step mechanism for combustion process. There was a stark difference in Stage A and Stage B of combustion process. The conversion values in Stage A varied from 0.05-0.3 while that in Stage B ranged between 0.4-0.9. It could be suggested that the combustion of volatiles and combustion of fixed carbon in char followed separate solid state reaction mechanism. To obtain a single value of each stage, an average of activation energy for individual stage was considered.

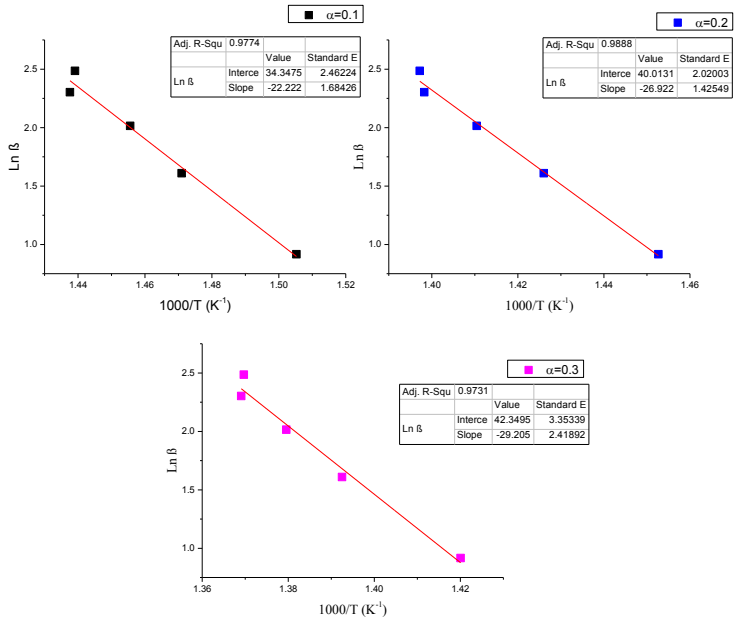

Figure 4.29: FWO plots for Stage A conversion of 425µm-0.85mm asphaltenes size pyrolyzed at 700˚C in furnace

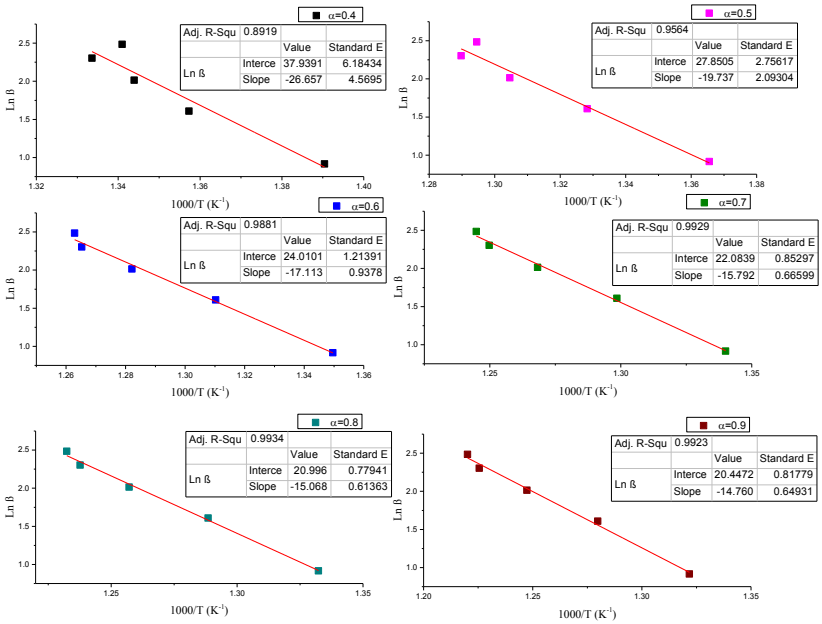

Figure 4.30: FWO plots for Stage B conversion of 425µm-0.85mm asphaltenes size pyrolyzed at 800˚C in furnace

With increase in pyrolysis temperature the activation energy for both the stages decreased when particle size was 425μm-0.85mm and 355-425μm. This indicated that combustion reactivity increased with pyrolysis temperature for the given size range. The morphology of chars obtained also suggested an increase in mesopores and macropores. However, the trend became reverse when the particle size reduced to 250-355μm. The reduction in char combustion reactivity with increasing pyrolysis temperature could be explained by massive loss in active sites (observed from FTIR). The decreasing reactivity might also be associated with progressive ordering of char at high pyrolysis temperatures leading to loss of micropore sites [105]. The average activation energy at different stages for all samples was tabulated in Table 4.3.

Table 4.3: Activation energy of all samples

Particle Size	Pyrolysis Temp(˚C)	Activation Energy(*kJ/mol*)	
		Stage A	Stage B
425μm-0.85mm	700	206.4	143.7
425μm-0.85mm	800	-	110.1
355-425μm	700	136.04	99.16
355-425μm	800	-	96.72
250-355μm	700	120.39	99.61
250-355μm	800	-	118.11

4.3.4. Comparison between Pyrolysis and Combustion rates

To obtain activation energy (E_a) of asphaltenes under inert (N_2) environment similar procedure was followed as in combustion experiments. The TG curve (Figure 4.31) indicated maximum conversion between 350-470˚C. The conversion for region varied from 0.05-0.5. Both KAS and FWO method was utilised to calculate the activation energy for conversion range of 0.05-0.5. The average value for FWO and KAS method was calculated to be 181.13 and 178.93*kJ/mol* respectively.

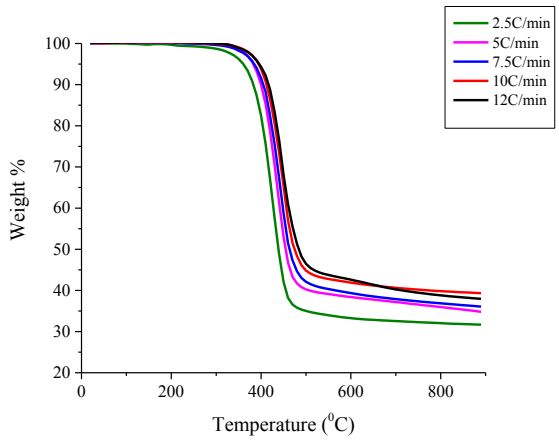

Figure 4.31: Weight loss curve for asphaltenes in N_2 atmosphere

The average value of Activation energy obtained for pyrolysis condition lied in the same range as Stage A for char combustion experiments. However the Stage B of char combustion experiments had lower E_a indicating that combustion rate was faster than the pyrolysis rate.

Table 4.4: Activation energy for asphaltenes obtained by FWO and KAS method for pyrolysis condition

α	Activation Energy(*kJ/mol*)	
	FWO method	KAS method
0.05	137.38	133.71
0.1	166.77	164.26
0.15	181.03	179.08
0.2	186.91	185.11
0.25	190.31	188.58
0.3	194.41	192.79
0.35	197.31	195.74
0.4	192.43	190.51
0.45	179.08	176.36
0.5	185.61	183.17

Chapter 5
CONCLUSION AND FUTURE RESEARCH

5.1. Conclusion

Following conclusion are drawn from the pyrolysis and partial oxidation experiments using entrained bed furnace:

- High furnace temperature and lower particle size lead to decrease in char yield. However the variation in yield for sizes 355-425μm and 250-355μm at 900°C was negligible. Particle size below 0.85mm at all furnace temperature had considerable impact on the char yield than higher size range.
- Both particle size and pyrolysis temperature influenced the structure of char. Char obtained from 1-1.4mm at 700°C had similar conformity as asphaltenes. Aliphatic and aromatic concentration decrease with furnace temperature, However there was modest increase in alkene and aromatics for char from 250-355μm size at 900°C.Oxygen distributed in form of aldehydes, ketones and ether decreased with pyrolysis temperature. Sulfur present in the form of thiocarbonyl also decreased with increase in pyrolysis temperature. Nitrogen present in asphaltenes rearranged as C≡N and made appearance only when the particle size was below 0.85mm.
- Chars in form of honeycomb and ribbed cenospheres were formed at temperatures above 800°C for particle sizes 355-425μm and 250-355μm. Cross-sectional SEM indicated fragmentation for particle size below 355µm at pyrolysis temperature of 900°C.
- The majority of ash compositions obtained from char during pyrolysis were dominated by V, Ni and Al (due to contamination). During ashing conditions most of the metals present converted into respective oxides. Evidence of Na, K, Ca and Cu presence might account for fouling and erosion in pipelines and furnace interiors. Retention of K and Na at high

pyrolysis temperature of 700°C and 900°C suggested existence of stable and complex inorganic forms. However, with increased pyrolysis temperature there was emission of mineral matter.

- Partial oxidation of 425μm-0.85mm asphaltenes at 700-900°C reiterated common conclusions. Increase in oxygen partial pressure at increasing pyrolysis temperature gave a better burnout. However minor aberration was noticed for 2% oxygen partial pressure with burnout percentages below that of 1% oxygen partial pressure. The char yield calculated from mass balance suggested a good carbon conversion.
- SEM analysis of char signified combustion of asphaltenes at furnace temperature of 900°C for 1-2% oxygen partial pressure. For partial pressure greater than 2% oxidation was conspicuous for all furnace temperatures.
- The combustion reactivity increased with pyrolysis temperature for particle size 355μm-0.85mm. However extensive loss of active sites(C=O, C=S) and structural ordering at high devolatilization temperature for 250-355μm size culminated in high activation energy and low reactivity.

5.2. Future Research

A more detailed study of transformation of Na, K, V and Ni during pyrolysis can be investigated. Retention of these elements in char, tar and gas phase can be figured out separately based on elemental analysis of char, tar and liquid collected in water scrubber. A sequential chemical extraction method can also be employed to determine mode of Na and K occurrence in char. A suitable mechanism can be developed to predict the products formed during pyrolysis and gasification. Ash behaviour can also be used to calculate alkali index, an indication for fouling and slagging propensity.

Reference

[1] Alberta Tourism, "Oil sands origin and location." [Online]. Available: http://history.alberta.ca/energyheritage/sands/origins/the-geology-of-the-oil-sands/the-location-of-oil-sands.aspx.

[2] Alberta Energy, "Oil sands: Facts and statistics." [Online]. Available: http://www.energy.alberta.ca/OilSands/791.asp.

[3] Canadian association of petroleum producers, "Canadian oil and natural gas."[Online].Available: http://oilsandstoday.ca/EnergyEconEnviron/Pages/default.aspx.

[4] S. Berryman, A. Garibaldi, and J. Straker, "A community approach for landscape planning," 2013.

[5] Mohammed Idris and L. Okoro, "A review on the effects of asphaltenes on petroleum processing," *Eur Chem Bulltein*, vol. 2, no. 6, pp. 393–396, 2013.

[6] G. Brons and J. M. Yu, "Solvent deasphalting effects on whole Cold Lake bitumen," *Energy Fuels*, vol. 9, no. 4, pp. 641–647, 1995.

[7] M. S. Rana, J. Ancheyta, S. K. Maity, and P. Rayo, "Hydrotreating of Maya crude oil :II. Generalised relationship between hydrogenolysis and hydrodeasphaltenization," *Petrol.SciTech*, vol. 25, no. 1–2, pp. 201–214, 2007.

[8] P. Wallace, kay. M. Anderson, and W. Preston, "Heavy oil upgrading by the separation and gasification of asphaltenes," in *Gasification Technologies Conference* , 1998.

[9] "Shell." [Online]. Available: www.shell.com/global/products-services/solutions-for-businesses/globalsolutions/gasification-licensing.html.

[10] C Higman and M. van der Burgt, *Gasification 2nd ed*. Gulf Professional Publishing/Elsevier, 2008.

[11] P. Basu, *Biomass Gasification and Pyrolysis: Practical Design*. 2010.

[12] C. D. Blasi, "Combustion and gasification rates of lignocellulosic chars," *Prog. Energy Combust. Sci.*, vol. 35, no. 2, pp. 71–104, 2009.

[13] P. Basu, "Burning rate of carbon in fluidized beds," *Fuel*, vol. 56, no. 4, pp. 390–392, 1977.

[14] I. Merdrignac and D. Espinat, "Physiochemical characterization of petroleum fractions: The state of art," *Oil Gas SciTech.-Rev.IFP*, vol. 62, no. 1, pp. 7–32, 2007.

[15] M. T. Martinez, A. M. Benito, and M. A. Callejas, "Thermal cracking of coal residues:Kinetics of asphaltene decomposition," *Fuel*, vol. 76, no. 9, pp. 871–877, 1997.

[16] L. Carbognani, M. Orea, and M. Fonseca, "Complex nature of separated solid phases from crude oils," *Energy Fuels*, vol. 13, no. 2, pp. 351–358, 1999.

[17] A. Demirbas, "Physical and chemical characterizations of asphaltenes from different sources," *Petrol.Sci.Tech*, vol. 20, no. 5–6, pp. 485–495, 2002.

[18] L. Z. Pillon, "Effect of experimental conditions and solvents on the precipitation and composition of asphaltenes," *Petrol.Sci.Tech*, vol. 19, no. 5–6, pp. 673–683, 2001.

[19] S. I. Andersen, "Dissolution of solid Boscan asphaltenes in mixed solvents," *Fuel Sci.Tech.Int*, vol. 12, no. 11–12, pp. 1551–1577, 1994.

[20] O. P. Strausz, P. Peng, and J. Murgich, "About the colloidal nature of asphaltenes and the MW of covalent monomeric units," *Energy Fuels*, vol. 16, no. 4, pp. 809–822, 2002.

[21] V. Calemma, P. Iwanski, M. Nali, R. Scotti, and L. Montanari, "Structural characterization of asphaltenes of different origins," *Energy Fuels*, vol. 9, no. 2, pp. 225–230, 1995.

[22] H. Groenzin and O. C. Mullins, "Asphaltene molecular size and structure," *J.Phys.Chem.A*, vol. 103, no. 50, pp. 11237–11245, 1999.

[23] H. Groenzin and O. C. Mullins, “Molecular size and structure of asphaltene from various sources,” *Energy Fuels*, vol. 14, no. 3, pp. 677–684, 2000.

[24] J. G. Speight and S. E. Moschopedis, “On the molecular structure of petroleum asphaltenes, in Chemistry of Asphaltenes,” *Adv. Chem. Ser. Am. Chem. Soc.*, vol. 195, pp. 1–15, 1981.

[25] B. Aguilera-Mercado, C. Herdes, J. Murgich, and E. A. Muller, “Mesoscopic simulation of aggregation of asphaltenes and resin molecules in crude oils,” *Energy Fuels*, vol. 20, no. 1, pp. 327–338, 2006.

[26] S. Zhao, L. S. Kotlyar, J. R. Woods, B. D. Sparks, K. Hardacre, and K. H. Chung, “Molecular transformation of Athabasca bitumen end-cuts during coking and hydrocracking,” *Fuel*, vol. 80, no. 8, pp. 1155–1163, 2001.

[27] E. Rogel and L. Carbognani, “Density estimation of asphaltenes using molecular dynamics simulations,” *Energy Fuels*, vol. 17, no. 2, pp. 378–386, 2003.

[28] K. L. Gawrys, P. M. Spiecker, and P. K. Kilpatrick, “The role of asphaltene solubility and chemistry on asphaltene aggregation:Conversion chemistry of petroleum residua,” *Am.Chem.Soc., Div.Petrol.Chem.-Prepr*, vol. 47, no. 4, pp. 332–335, 2002.

[29] J. G. Speight, “Chemical and physical studies of petroleum asphaltenes,” *Asph. Asph.*, pp. 35–37, 1994.

[30] J. M. Sheremata, M. R. Gray, H. D. Dettman, and W. C. McCaffery, “Quantitative molecular representation and sequential optimization of Athabasca asphaltenes,” *Energy Fuels*, vol. 18, no. 5, pp. 1377–1384, 2004.

[31] J. Murgich, J. Rodriguez, and Y. Aray, “Molecular recognition and molecular mechanics of micelles of some model asphaltenes and resins,” *Energy Fuels*, vol. 10, no. 1, pp. 68–76, 1996.

[32] G. W. Zajac, N. K. Sethi, and J. T. Joseph, “Molecular imaging of petroleum asphaltenes by scanning tunneling microscopy:Verification of

structure from 13C and proton nuclear magnetic resonance data," *Scann.Microscopy*, vol. 8, no. 3, pp. 463–470, 1994.

[33] G. W. Zajac, N. K. Sethi, and J. T. Joseph, "Maya petroleum asphaltene imaging by scanning tunneling microscopy:Verification of structure from 13C and proton nuclear magnetic resonance," *Am.Chem.Soc., Div.Fuel Chem*, vol. 42, no. 2, pp. 423–426, 1997.

[34] S. I. Andersen, J. O. Jensen, and J. G. Speight, "X-ray diffraction of subfractions of petroleum asphaltenes," *Energy Fuels*, vol. 19, no. 6, pp. 2371–2377, 2005.

[35] E. Buenrostro-Gonzalez, M. Espinosa-Pena, S. I. Andersen, and C. Lira-Galeana, "Characterization of asphaltenes and resins from problematic Mexican crude oils," *Petrol.Sci.Tech*, vol. 19, no. 3–4, pp. 299–316.

[36] P. Luo and Y. Gu, "Effects of asphaltene content on the heavy oil viscosity at different temperatures," *Fuel*, vol. 86, no. 7–8, pp. 1069–1078, 2007.

[37] S. Peramanu, B. B. Pruden, and P. Rahimi, "Molecular weight and specific gravity distributions for Athabasca and Cold Lake bitumens and their saturate, aromatic, resin and asphaltene fraction," *Ind.Eng.Chem.Res*, vol. 38, no. 8, pp. 3121–3130, 1999.

[38] C. H. Whitson, "Characterizing hydrocarbon plus fractions," *SPE J.*, vol. 23, pp. 683–694, 1983.

[39] H. W. Yarranton and J. H. Masliyah, "Molar mass distribution and solubility modeling of asphaltenes," *AICHE J.*, vol. 42, no. 12, pp. 3533–3543, 1996.

[40] S. I. Andersen and K. S. Birdi, "Influence of temperature and solvent on the precipitation of asphaltenes," *Fuel Sci.Tech.Int*, vol. 8, no. 6, pp. 593–615, 1990.

[41] T. A. Al-Sahhaf, M. A. Fahim, and A. S. Elkilani, "Retardation of asphaltene precipitation by addition of toluene, resins, deasphalted oil and surfactants," *Fluid Phase Equilib*, vol. 194197, pp. 1045–1057, 2002.

[42] J. G. Reynolds, “Trace metals in heavy crude oil and tar and bitumens,” *Eastern Oil Shale symposium*. Lexington,KY, 1990.

[43] D. L. Mitchell and J. G. Speight, “Solubility of asphaltenes in hydrocarbon solvents,” *Fuel*, vol. 52, no. 2, pp. 431–434, 1973.

[44] L. W. Corbett and U. Petrossi, “Differences in distillation and solvent separated asphalt residua,” *Ind.Eng.Chem.Proc.Des.Dev*, vol. 17, no. 4, pp. 342–346, 1978.

[45] B. J. Fuhr, C. Cathrea, L. Coates, H. Kalra, and A. I. Majeed, “Properties of asphaltenes from a waxy crude,” *Fuel*, vol. 70, no. 11, pp. 1293–1297, 1991.

[46] Y. F. Hu and T. M. Guo, “Effect of temperature and molecular weight of n-alkane precipitants on asphaltene precipitation,” *Fluid Phase Equilib*, vol. 192, no. 1–2, pp. 13–25, 2001.

[47] J. Ancheyta, G. Centeno, F. Trejo, G. Marroquin, J. A. Garcia, E. Tenorio, and A. Torres, “Extraction and characterization of asphaltenes from different crude oils and solvents,” *Energy Fuels*, vol. 16, no. 5, pp. 1121–1127, 2002.

[48] G. Centeno, F. Trejo, J. Ancheyta, and A. Carlos, “Precipitation of asphaltenes from Maya crude in a pressurized system,” *J.Mex.Chem.Soc*, vol. 48, no. 3, pp. 186–195, 2004.

[49] G. Gonzalez, M. A. Sousa, and E. F. Lucas, “Asphaltenes precipitation from crude oil and hydrocarbon media,” *Energy Fuels*, vol. 20, no. 6, pp. 2544–2551, 2006.

[50] L. H. Ali and K. A. Al-Ghannam, “Investigations into asphaltenes in heavy crude oils.I. Effect of temperature on precipitation by alkane solvents,” *Fuel*, vol. 60, no. 1, pp. 1043–1046, 1981.

[51] O. Leon, E. Rogel, J. Espidel, and G. Torres, “Structural characterization and self association of asphaltenes of different origins.,” *AIChE Spring National Meeting*. Houston, pp. 37–43, 1999.

[52] M. N. Siddiqui, “Infrared study of hydrogen bond types in asphaltenes.,” *Petrol.Sci.Tech*, vol. 21, no. 9–10, pp. 1601–1615, 2003.

[53] S. Mitra-Kirtley, O. C. Mullins, J. V Elp, S. J. George, J. Chen, and S. P. Cramer, “Determination of nitrogen chemical structures inpetroleum asphaltenes using XANES spectroscopy,” *J.Am.Chem.Soc*, vol. 115, no. 1, pp. 252–258, 1993.

[54] J.-M. Schmitter, I. Ignatiadis, M. Dorbon, M. Arpino, G. Guiochon, H. Toulhoat, and A. Hue, “Identification of nitrogen bases in a coker gas oil and influence of catalytic hydrotreatment on their composition,” *Fuel*, vol. 63, no. 4, pp. 557–564, 1984.

[55] M. Dorbon, I. Ignatiadis, J.-M. Schmitter, M. Arpino, G. Guiochon, H. Toulhoat, and A. Huc, “Identification of carbazoles and benzocarbazoles in a coker gas oil and influence of catalytic hydrotreatment on their distribution,” *Fuel*, vol. 63, no. 4, pp. 565–570, 1984.

[56] P. K. Dutta and R. J. Holland, “Acid-Base characteristics of petroleum asphaltenes as studied by non-aqueous potentiometric titrations,” *Fuel*, vol. 63, no. 2, pp. 197–201, 1984.

[57] A. Jada and M. Salou, “Effects of asphaltene and resin contents of the bitumens on the water-bitumen interface properties,” *J.Petrol.Sci.Eng*, vol. 33, no. 1, pp. 185–193, 2002.

[58] H. V Drushel, “Trace sulfur determination in petroleum fractions,” *Anal.Chem.*, vol. 50, no. 1, pp. 76–81, 1978.

[59] S. R. Kelemen, G. N. George, and M. L. Gorbaty, “Direct determination and quantification of sulphur forms in heavy petroleum and coals: 1. The x-ray photoelectron spectroscopy(XPS) approach,” *Fuel*, vol. 69, no. 8, pp. 939–944, 1990.

[60] O. C. Mullins, “Sulfur and nitrogen molecular structures in asphaltenes and related materials quantified by XANES spectroscopy,” in *Asphaltenes: Fundamentals and Applications*, New York: Plenum Press, 1995.

[61] K. D. Rose and M. A. Francisco, “Characterization of acididc heteroatoms in heavy petroleum fractions by phase-transfer methylation and NMR spectroscopy ,” *Energy Fuels*, vol. 1, no. 3, pp. 233–239, 1987.

[62] R. George, S. Ritchie, R. S. Roche, and W. Steedman, “Pyrolysis of Athabasca tar sands: Analysis of the condensable products from asphaltene,” *Fuel*, vol. 58, no. 7, pp. 523–530, 1979.

[63] Z. Frakman, T. M. Ignasiak, E. M. Lown, and O. P. Strausz, “Oxygen compounds in Athabasca asphaltene,” *Energy Fuels*, vol. 4, no. 3, pp. 263–270, 1990.

[64] B. K. Wilt, W. T. Welch, and J. G. Rankin, “Determination of asphaltenes in petroleum crude oils by Fourier transform infrared spectroscopy,” *Energy Fuels*, vol. 12, no. 5, pp. 1008–1012, 1998.

[65] H. W. Yarranton, H. Alboudwarej, and R. Jakher, “Investigation of asphaltene association with vapor pressure osmometry and interfacial tension measurements ,” *Ind.Eng.Chem.Res.*, vol. 39, no. 8, pp. 2916–2924, 2000.

[66] J. Yu, J. Lucas, and T. F. Wall, “Formation of the structure of chars during devolatilization of pulverized coal and its thermoproperties: A review,” *Prog. Energy Combust. Sci.*, vol. 33, pp. 135–170, 2007.

[67] A. V. Bridgwater, D. Meier, and D. Radlein, “An overview of fast pyrolysis of biomass,” *Org. Geochem.*, vol. 30, pp. 1479–1493, 1999.

[68] G. R. Gavalas, *Coal Pyrolysis*. Coal Science and Technology,Elsevier, 1982.

[69] M. S. Oh, W. A. Peters, and J. B. Howard, “An experimental and modeling study of softening coal pyrolysis,” *AICHE J.*, vol. 35, no. 5, pp. 775–792, 1989.

[70] H. Y. Park and D. H. Ahn, “Gasification kinetics of five coal chars with CO2 at elevated pressure,” *Korean J.Chem.Eng*, vol. 24, no. 1, pp. 24–30, 2007.

[71] A. D. Koranyi, “The relationship between specific reactivity and the pore structure of coal chars during gasifiaction,” *Carbon N. Y.*, vol. 27, no. 1, pp. 55–61, 1989.

[72] K. Zygourakis, “Effect of pyrolysis conditions on the macropore structure of coal derived chars,” *Energy Fuels*, vol. 7, pp. 33–41, 1993.

[73] H. Wu, G. Bryant, and T. F. Wall, “The effect of pressure on ash formation during pulverized coal combustion,” *Energy Fuels*, vol. 14, no. 4, pp. 745–750, 2000.

[74] B. F and P. R, “Characterization of asphaltenes by pyrolysis and chromatography,” *J. Anal. Appl. Pyrolysis*, vol. 7, pp. 121–135, 1984.

[75] T. Daniel, Y. Muzaffer, N. Matthew, N. Abhash, K. Michael, and K. Simon, “Asphaltene and resid pyrolysis: Effect of reaction environment,” *Fuel Sci.Tech.Int*, vol. 10, no. 7, pp. 1161–1179, 1992.

[76] J. Douda, L. E. Ma, R. Alvarez, L. C. Franco, and J. Ascension Montoya de la Fuente, “Pyrolysis applied to the study of a Maya asphaltene,” *J. Anal. Appl. Pyrolysis*, vol. 7, pp. 601–612, 2004.

[77] Y. Zhao, F. Wei, and Y. Yu, “Effects of reaction time and temperature on carbonization in asphaltene pyrolysis,” *J. Pet. Sci. Eng.*, vol. 74, pp. 20–25, 2010.

[78] W.-C. Ricky Chan, M. Kelbon, and B. Krieger-Brockett, “Single PArticle Biomass Pyrolysis: Correlations of Reaction Products with Process Conditions,” *Ind.Eng.Chem.Res.*, vol. 27, pp. 2261–2275, 1988.

[79] M. Momeni, “Fundamental study of single biomass particle combustion,” Aalborg University, Denmark, 2012.

[80] P. Moszkowicz and L. Witzel, “Modelling of very fast pyrolysis of heavy fuel oil droplets,” *Chem. Eng. Sci.*, vol. 51, no. 17, pp. 4075–4086, 1996.

[81] R. Kalpokaite-Dichkuvene and G. Stravinskas, “Behavior of a fuel oil droplet on a hot surface,” *J. Eng. Phys. Thermophys.*, vol. 79, no. 1, 2006.

[82] K. D. Bartle, J. M. Jones, A. R. Lea-Langton, M. Pourkashanian, A. B. Ross, J. S. Thillaimuthu, P. R. Waller, and A. Williams, "The combustion of droplets of high asphaltene heavy oils," *Fuel*, vol. 103, pp. 835–842, 2013.

[83] A. Paakkonen, A. Peltola, A. Pitkanen, R. Makiranta, A. Saario, and A. Oksanen, "Developing and testing characterization methods for droplet combustion-Part I," *Arch. Combust.*, vol. 30, no. 4, 2010.

[84] B. Moghtaderi, "A study on the char burnout characteristics of coal and biomass blends," *Fuel*, vol. 86, pp. 2431–2438, 2007.

[85] J. Riaza, L. Alvarez, M. V. Gil, C. Pevida, J. J. Pis, and F. Rubeira, "Effect of oxy-fuel combustion with steam addition on coal ignition and burnout in an entrained flow reactor," *Energy*, vol. 36, pp. 5314–5319, 2011.

[86] B. Arias, C. Pevida, F. Rubeira, and J. J. Pis, "Effect of biomass blending on coal ignition and burnout during oxy-fuel combustion," *Fuel*, vol. 87, pp. 2753–2759, 2008.

[87] T. Ito, M. Takafuji, T. Suda, and T. Fujimori, "Fundamental study of the pulverized coal char combustion in oxyfuel mode with drop tube furnace," in *Springer*, 2013, pp. 605–609.

[88] X. Li, R. . Rathnam, J. Yu, Q. Wang, T. F. Wall, and C. Meesri, "Pyrolysis and combustion charcteristics of an Indonesian low-rank coal under O2/N2 and O2/CO2 conditions," *Energy Fuels*, vol. 24, pp. 160–164, 2010.

[89] A. G. Borrego, E. Osotio, M. D. Casal, and A. C. F. Vilela, "Coal char combustion under a CO2 rich atmosphere: Implications for pulverised coal injection in a blast furnace," *Fuel Process. Technol.*, vol. 89, no. 11, pp. 1017–1024, 2008.

[90] H. Cai, A. J. Guell, I. N. Chatzakis, J.-Y. Lim, R. Dugwell, and R. Kandiyoti, "Combustion reactivity and morphological change in col chars: effect of pyrolysis temperature, heating rate and pressure," *Fuel*, vol. 75, no. 1, pp. 15–24, 1996.

[91] H. Haykiri-Acma, A. Ersoy-Mericboyu, and S. Kucukbayrak, "Effect of mineral matter on the reactivity of lignite chars," *Energy Convers. Manag.*, vol. 42, no. 2001, pp. 11–20, 2001.

[92] A. Khawan and R. D. Flanagan, "Solid-State kinetic Models: Basic and Mathematical Fundamentals," *J.Phys.Chem.B*, vol. 110, no. 35, pp. 17315–17328, 2006.

[93] A. Aboulkas and K. El Harfi, "Study of the kinetics and mechanisms of thermal decomposition of moroccan tarfaya oil shale and its kerogen," *Oil Shale*, vol. 25, no. 4, pp. 426–443, 2008.

[94] O. Onay, "Influence of pyrolysis temperature and heating rate on the production of bio-oil and char from safflower seed by pyrolysis, using a well swept fixed bed reactor," *Fuel Process. Technol.*, vol. 88, pp. 523–531, 2007.

[95] F. Meng, J. Yu, A. Tahmasebi, Y. Han, H. Zhao, J. Lucas, and T. F. Wall, "Characteristics of chars from low temperature pyrolysis of lignite," *Energy Fuels*, vol. 28, pp. 275–284, 2014.

[96] N. Olukcu, J. Yanik, M. Saglam, and M. Yuksel, "Liquefaction of beypazari oil shale by pyrolysis," *J. Anal. Appl. Pyrolysis*, vol. 64, pp. 29–41, 2002.

[97] C. zhu Li, "Conversion of coal-N and coal-S during pyrolysis, gasification and combustion," in *Advances in the science of Victorian brown coal*, Elsevier, 2004.

[98] K. Bukka, J. D. Miller, and A. G. Obladt, "Fractionation and characterization of Utah tar sand viscosity bitumens: Influence of chemical composition on bitumen," *Energy Fuels*, vol. 5, pp. 333–340, 1991.

[99] M. Al-Wabel, A. Al-Omran, A. El-Naggar, Ma. Nadeem, and A. R. A. Usman, "Pyrolysis temperature induced charges in characteristics and chemical composition of biochar produced from conocarpus wastes," *Bioresour. Technol.*, vol. 131, pp. 374–379, 2013.

[100] J. Gary, G. E. Handwerk, and M. J. Kaiser, *Petroleum refining technology and economics*, 5th ed. Taylor and Francis group, 2007.

[101] S. Jayanti, K. Maheswaran, and V. Saravanan, "Assessment of the effect of high ash content in pulverised coal combustion," *Appl. Math. Model.*, vol. 31, no. 5, pp. 934–953, 2007.

[102] X. Wei, J. Huang, T. Liu, Y. Fang, and Y. Wang, "Transformation of alkali metals during pyrolysis and gasification of a lignite," *Energy Fuels*, vol. 22, pp. 1840–1844, 2008.

[103] D. J. Lane, P. J. va. Eyk, P. J. Ashman, C. W. Kwong, R. de Nys, D. A. Roberts, A. J. Cole, and D. M. Lewis, "Release of Cl,S,P,K and Na during thermal conversion of algal biomass," *Energy Fuels*, vol. 29, pp. 2542–2554, 2015.

[104] M. V. Gil, M. D. Casal, C. Pevida, J. J. Pis, and F. Rubeira, "Thermal behaviour and kinetics of coal/biomass blends during co-combustion," *Bioresour. Technol.*, vol. 101, pp. 5601–5608, 2010.

[105] N. Mahapatra, "Pyrolysis of asphaltenes in an atmospheric entrained flow reactor: A study on gasification reactivity and properties of chars," University of Alberta, 2014.

[106] M. . Diallo, T. Cagin, J. . Faulon, and W. . Goddard III, "Thermodynamic properties of asphaltenes: A predictive approach based on computer asssited structure elucidation and atomistic simulations," *Asph. Asph. 2. Dev. Pet. Sci.*, vol. 40B, 2000.

[107] H. Zhu, J. Jing, J. Chen, Q. Li, and X. Yu, "Simulations of deposition rate of asphaltene and flow properties of oil-gas-water three phase flow in submarine pipelines by CFD," *IEEE*, 2010.

APPENDIX

A.1 Operation of Furnace

The home page of the Thermolyne furnace consists of actual temperature, Page button, refresh button and arrow keys. OP1 illuminates when the output is heating while OP2 illuminates when it's normally cooling.

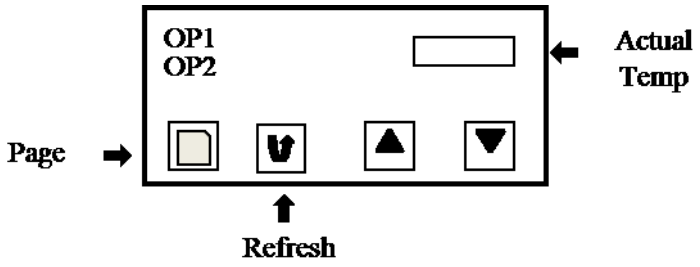

To adjust the temperature the upward or downward arrow was held and released quickly. The maximum temperature the furnace could attain was set at 1000˚C, so precaution was taken to maintain operating temperature below 1000˚C. The next step involved in choosing mode of heating (OPt) and fixing a heating rate (SPrr). Following steps were followed to achieve the objective:

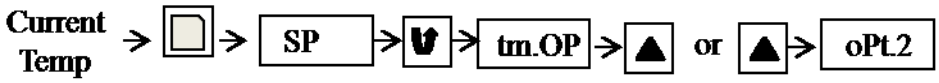

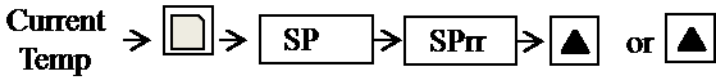

Thermolyne offered five modes of heating with OPt.1 and OPt.2 being used widely. OPt.1 caused cooling of the furnace after dwelling the setpoint for certain time while OPt.2 maintained the set temperature indefinitely. After setting required temperature, heating rate and mode of heating following step was executed.

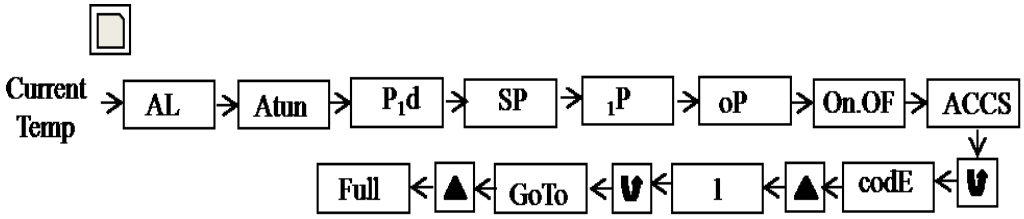

Finally to start the furnace heating "Auto" mode was chosen and this was verified by appearance of "OP1" in the home screen. To stop heating similar step was followed as below but "Man" was chosen instead of "Auto".

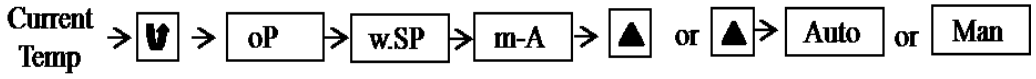

For sudden ramp in temperature during heating, the furnace was immediately set to "Man" mode.

A.2 Calibration of Furnace

The temperature of furnace was calibrated by using 20 inch K-type thermocouple. The thermocouple marked at intervals of 5*cm* was allowed into the furnace set at 600°C, 700°C and 800°C with nitrogen flow in. It was noticed that the furnace was heated efficiently from 20-40*cm* only. At higher set temperatures the actual temperature of the tube was closer to desired values. Thus all experiments were carried out at 50°C higher than the required temperature for efficient heating.

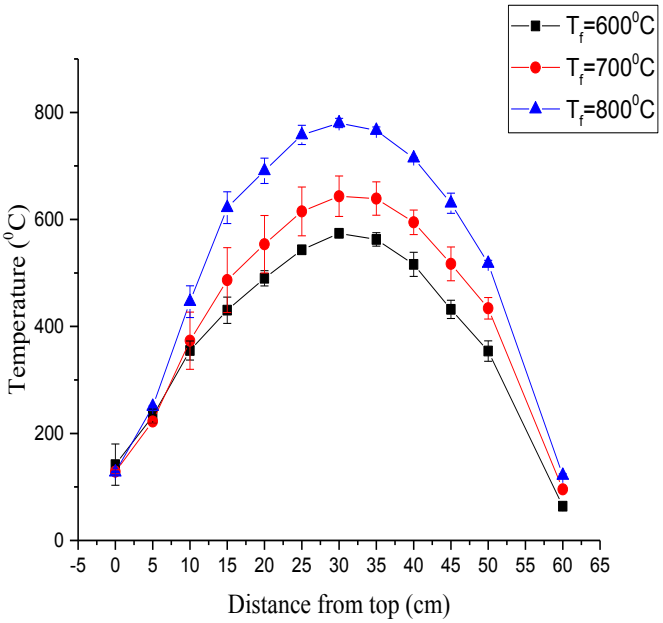

Figure A.1: Variation of temperature along DTF

A.3. Particle Temperature

To calculate the temperature attained by single particle during pyrolysis MATLAB code was executed with following assumptions:

1. The temperature of the furnace T_w did not depend on the heat transfers with the gas or the droplet. The thermal profile was determined experimentally.
2. To simplify the problem into one dimensional study, the particle was considered to be spherically symmetric.
3. Physico-thermal properties of the surrounding gas were considered to be temperature independent.
4. The gas moved in a plug flow pattern. For a section of given distance x, the gas temperature T_g and wall temperature T_w was considered to be constant.
5. The gas was transparent to radiation.
6. All heat transfers with the particle took place at the surface.

7. Temperature gradient within the particle was neglected.

Heat transfers

1) The heat transfer between the furnace wall and the particle was radiative at the surface of particle. The energy flow was given by:-

$$Q_r = \varepsilon_p A_p \sigma (T_w^4 - T_p^4) \quad \text{(A.1)}$$

2) The heat transfer between the gas and particle was convective in nature and took place at the surface of the particle. The energy flow was illustrated by:-

$$Q_c = hA_p(T_g - T_p) \quad \text{(A.2)}$$

The heat transfer coefficient 'h' was dependent on the flow around the particle

$$Nu = \frac{hd_p}{\lambda_g} = 2 + 0.6Re^{0.5}Pr^{0.33} \quad \text{(A.3)}$$

Heat transfer within the particle was neglected and this could be justified by calculation Biota number (Bi).

$$Bi = \frac{hL_c}{k_p} = \frac{hV_p}{k_p A_p} = \frac{hr_p}{3k_p} \quad \text{(A.4)}$$

Biot number provided the measure of temperature drop in a solid relative to temperature difference between surface and fluid. When Bi<<1, the resistance to conduction was much less than resistance to convection across the fluid boundary.

3) Heat of reaction in the particle is given by:-

$$Q_p = -\frac{dm_p}{dt} H = -k[mp - (1 - f_v)m_{p0}]H \quad \text{(A.5)}$$

where,

$$k = Aexp(\frac{E_a}{RT_p}) \quad \text{(A.6)}$$

The overall relation for particle temperature calculation was given by:

$$m_p c_p \frac{dT_p}{dt} = hA_p\left(T_g - T_p\right) + \varepsilon_p A_p \sigma\left(T_w^4 - T_p^4\right) - k[m_p - (1 - f_v)m_{p0}]H \quad \text{(A.7)}$$

Identification of model parameters:

c_p : Specific heat of the particle = 1597.45 *J/kgK* [106]

A_p : Area of the particle

ρ_p : Density of the particle = 1200 kg/m^3

ε_p : Emissivity of particle = 0.9

λ_g : Thermal conductivity of nitrogen = 0.024*W/mK* [107]

σ : Stefan's constant = $5.67*10^{-8}$ W/m^2K^4

k_p : Thermal conductivity of particle = 1.7 *W/mK*

H : Heat of pyrolysis = 19.8*kJ/kg*

d_p : Diameter of the particle = average diameter for particle ranges

T_w : Furnace wall temperature = 873, 973, 1073 and 1173*K*

T_g : Gas/Nitrogen temperature=723, 903,1023K and 1153*K*

It was estimated that the larger particle sizes took more than 20*s* to reach the gas temperature. However the residence time was limited to 3-4*s* with duration in efficient heating zone as lower than 2*s*. Hence, the inappropriate heating and reaction at lower temperatures and larger particle sizes could be accounted for. With furnace temperature of 900°C and particle sizes lower than 450μm the heat up time for particles was reduced to below 2*s* giving ample time for reaction, hence better volatile yield. The temperature attained by the particles at their respective residence time was tabulated in Table A.1.

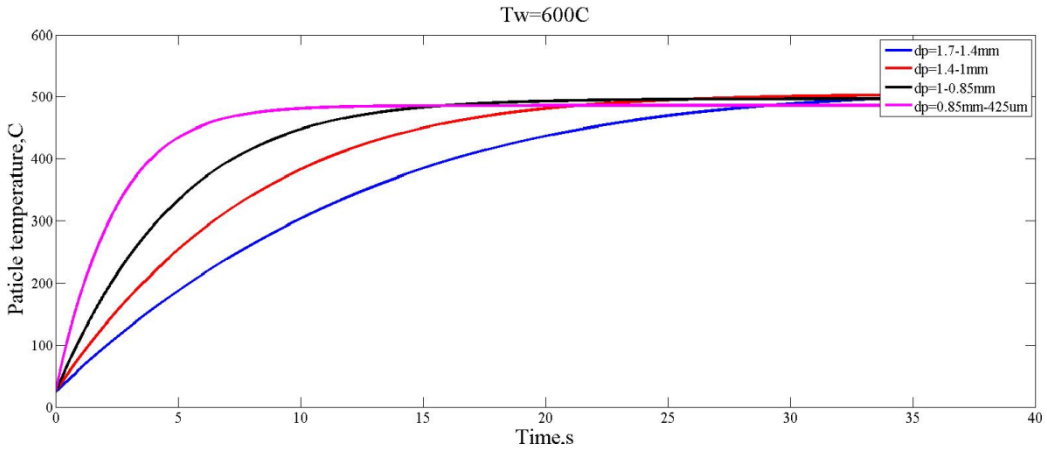

Figure A.2: Temperature attained by high size particles at 600°C

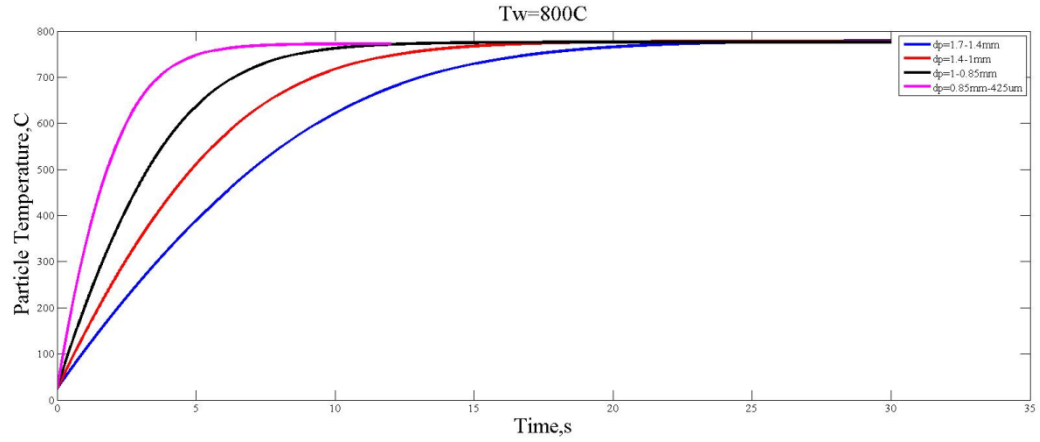

Figure A.3: Temperature attained by high size particles at 800°C

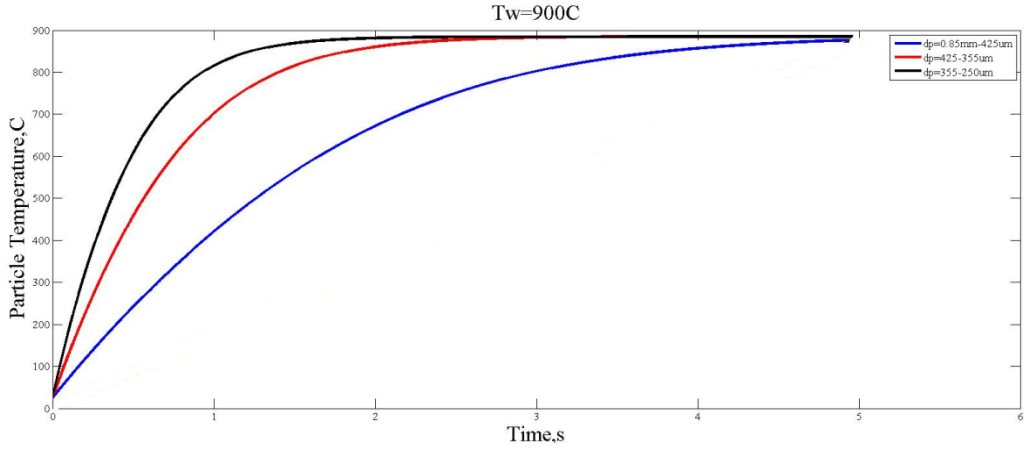

Figure A.4: Temperature attained by low size particles at 900°C

Table A.1: Table for particle temperature at residence time inside the furnace

Wall Temp (˚C)	Residence Time (sec)	Particle Temperature ˚C					
		1.4-1.7*mm*	1-1.4*mm*	0.85-1*mm*	425μm-0.85*mm*	355-425μm	250-355μm
600	3.69	194.38	204.8	277.78	390.9	-	-
700	3.31	234.12	283.47	385	541	641	645
800	3.01	267.5	363.68	486.9	665	772	777
900	2.75	-	-	-	779	881	884

A.4. Repeatability of Experiments

Pyrolysis experiments at all particle sizes and temperature were repeated thrice to confirm the repeatability. Similarly the partial combustion experiments in drop tube furnace as well as the kinetics experiments in TGA were conducted twice to account for accuracy of the present work. The error for yield in plot below varied from $\pm$0.8% - $\pm$4.8%.

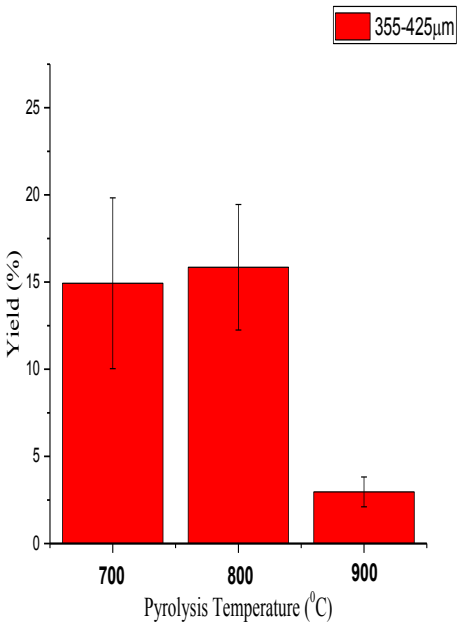

Figure A.5: Error in obtaining char yield

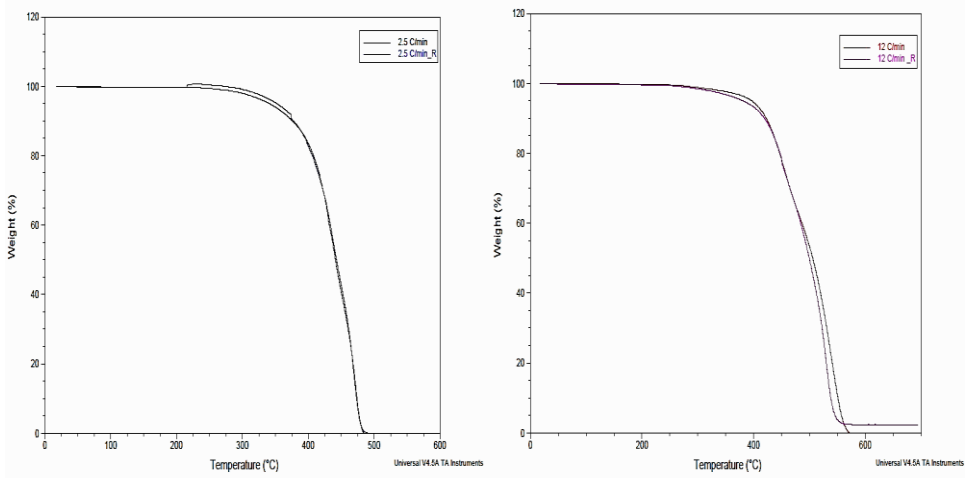

Figure A.6: Repeatability of TG curves for 250-355µm 700°C char at low and high heating rates

A.5. Determination of Order of Pyrolysis Kinetics

In order to determine the kinetic model of thermal degradation, Coats-Redfern method was chosen. Apparent activation energy (E_a) was calculated for $10^{\circ}C/min$ heating rate by fitting $Lng(\alpha)/T^2$ vs. 1/T plots. The best regression coefficient (R^2) indicated that the thermal degradation followed the particular reaction model. To unravel the degradation mechanism, E_a and regression coefficients for various reaction models were tabulated below.

Table A.2: Apparent activation energies and R^2 for various models

Reaction Models	Activation Energy (*kJ/mol*)	R^2
P2	52.32	0.9665
P3	30.94	0.9571
P4	20.25	0.9436
A2	60.53	0.9786
A3	36.41	0.9734
A4	24.36	0.9664
R2	124.42	0.9793
R3	127.18	0.9798
D1	244.74	0.9759

D2	255.04	0.9789
D3	258.75	0.9789
D4	258.75	0.9789
F1	132.89	0.9874
F2	**171.66**	**0.9888**
F3	151.28	0.9824

Activation energy obtained in case of second order reaction (F2) was comparable to that from KAS and FWO method. Moreover, F2 model illustrated maximum agreement with high regression coefficient. Thus, $f(\alpha)$ and $g(\alpha)$ could be considered as $(1-\alpha)^2$, $(1-\alpha)^{-1}-1$ respectively for calculation of frequency factor(A) in rate equation from KAS and FWO method.

Table A.3: E_a and A calculated from KAS and FWO method

α	Ea(*kJ/mol*)		A(min^{-1})	
	KAS	FWO	KAS	FWO
0.05	133.71	137.38	5.39E+8	1.31E+9
0.1	164.26	166.77	1.51E+11	2.64E+11
0.15	179.08	181.03	2.11E+12	3.22E+12
0.2	185.11	186.91	5.89E+12	8.62E+12
0.25	188.58	190.31	1.04E+13	1.5E+13
0.3	192.79	194.41	2.10E+13	2.95E+13
0.35	195.74	197.31	3.35E+13	4.63E+13
0.4	190.51	192.43	1.27E+13	1.88E+13
0.45	176.36	179.08	1.02E+12	1.79E+12
0.5	183.17	185.61	3.05E+12	5E+12

A.6. Determination of Mineral Matter in Char by XRF

Low ash content in asphaltenes as well as char obtained from pyrolysis of asphaltenes made the data collected from ICP-MS inaccurate. The results

obtained from ICP-MS should be used for qualitative purposes and not for quantitative comparisons. Hence, XRF analysis was carried out to elucidate better understanding of mineral matter content in char obtained.

Al and Fe were contaminants and their presence should not be compared. V and Ni were highest components of mineral matter in both asphaltenes and char. Good fraction of P and S indicated that the metal were present in form of phosphates and sulfides. K, Ca, Ti and Zr also existed in char at pyrolysis temperatures of 900˚C. Some fraction of Si presence might be due to the contamination from fiberfrax and K-wool insulation. For both the particle sizes the mineral matter like K, Ca, V, Ni, P, Zr decreases with pyrolysis temperature. S content increases with temperature for 425μm-0.85mm asphaltenes size which was corroborated by FTIR analysis. With particle size 355-425μm, the mineral content in char was lower than 425μm-0.85mm size fraction. This could be attributed to the higher heating rate in small size particles, thereby better metal release into gaseous phase.

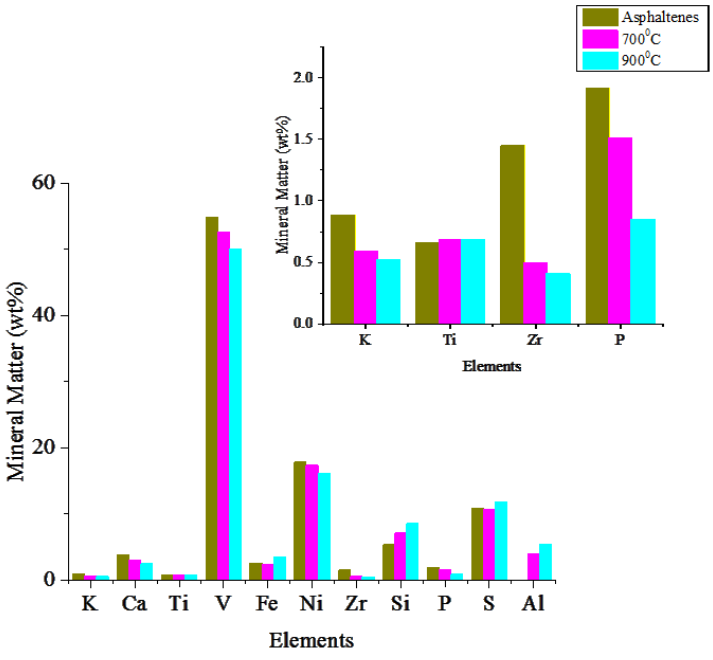

Figure A. 7: Metal content in 425µm-0.85mm size char ash from XRF

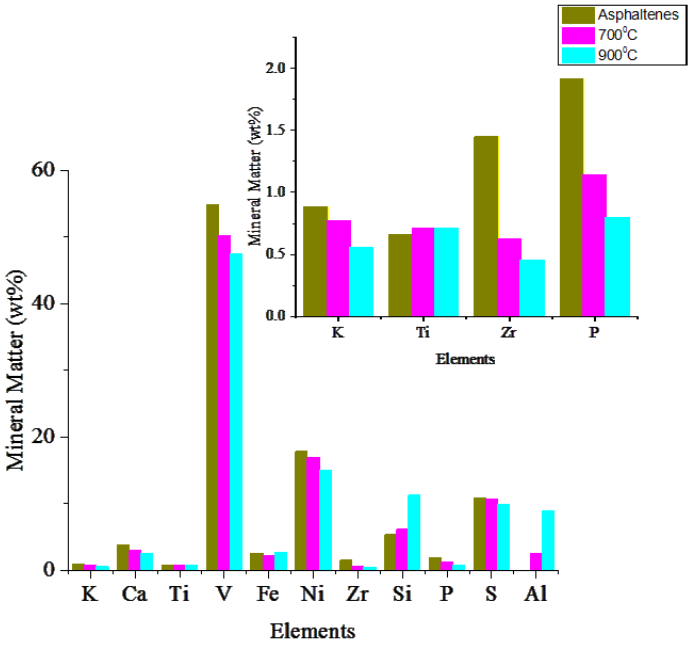

Figure A. 8: Metal content in 355-425µm size char ash from XRF